NATIONAL ADVISORY COMMITTEE FOR AERONAUTICS

TECHNICAL NOTE

No. 1048

TWO-DIMENSIONAL WIND-TUNNEL INVESTIGATION OF LOW-DRAG VERTICAL-TAIL, HORIZONTAL-TAIL, AND WING SECTIONS EQUIPPED WITH SEALED INTERNALLY BALANCED CONTROL SURFACES

By Albert L. Braslow

Langley Memorial Aeronautical Laboratory
Langley Field, Va.

Washington
April 1946

NATIONAL ADVISORY COMMITTEE FOR AERONAUTICS

TECHNICAL NOTE NO. 1048

TWO-DIMENSIONAL WIND-TUNNEL INVESTIGATION OF LOW-DRAG VERTICAL-TAIL, HORIZONTAL-TAIL, AND WING SECTIONS EQUIPPED WITH SEALED INTERNALLY BALANCED CONTROL SURFACES

By Albert L. Braslow

SUMMARY

A two-dimensional wind-tunnel investigation was made of three low-drag airfoil sections equipped with sealed internally balanced control surfaces designed for use as vertical-tail, horizontal-tail, and wing sections. The tests included determination of control-surface effectiveness and hinge moments and airfoil section drag characteristics. Balance pressures were also measured for use in estimating the hinge-moment characteristics of the control surfaces with any amount of sealed internal balance.

Sharp irregularities occurred in the variation of the control-surface section hinge-moment coefficient with airfoil section angle of attack, which were probably caused by sudden movements in transition along the surfaces of all three airfoils at the extremities of the low-drag range. Tests of the vertical-tail section indicated that these irregularities were reduced in magnitude when transition was fixed at a forward chordwise position but were not entirely removed until transition was fixed at the airfoil leading edge. An estimated variation of aileron wheel force with wing-tip helix angle for an assumed airplane indicated that no unusual aileron wheel-force characteristics would be caused by the irregularities in the two-dimensional hinge-moment characteristics. Sudden movements in transition along the surfaces of vertical-tail or horizontal-tail sections, however, would probably cause sudden changes in rudder or elevator hinge moments.

INTRODUCTION

The recent trend toward the use of large high-speed airplanes has imposed upon the airplane designer the problem of obtaining adequate control effectiveness without excessive control forces while securing low values of airfoil drag and high values of critical Mach number. Data for use by the designer in the prediction of low-drag-wing characteristics are available but only a limited amount of data on two-dimensional aerodynamic characteristics of control surfaces on low-drag airfoils is available. An investigation was made in the Langley two-dimensional low-turbulence pressure tunnel of two NACA 64-series-type airfoils and one NACA 7-series-type airfoil equipped with sealed internally balanced control surfaces to provide additional data on two-dimensional characteristics of control surfaces on low-drag airfoils. The 64-series-type airfoils were intended for use as tail surfaces and were equipped with a rudder and elevator of 0.40 and 0.35 airfoil chord, respectively. The 7-series-type airfoil was fitted with an aileron of 0.22 airfoil chord.

The tests, which were made at Reynolds numbers of 3×10^6, 6×10^6, and 9×10^6, included the determination of control-surface effectiveness and hinge moments and airfoil section drag characteristics. The pressure differences across the control-surface seals were also obtained for use in estimating the hinge-moment characteristics of the control surfaces with any amount of sealed internal balance.

SYMBOLS AND COEFFICIENTS

The symbols and coefficients used in the presentation of results are defined as follows:

a_o airfoil section angle of attack, degrees

c chord of airfoil with control surface neutral; measured along maximum length line

c_x chord of control surface measured from hinge axis to trailing edge

c_b	chord of overhang from control-surface hinge axis to middle of gap seal
δ_x	control-surface deflection with respect to airfoil; positive when trailing edge is deflected downward
R	Reynolds number
q_o	free-stream dynamic pressure
b	total wing span
b_a	span of one aileron
$\overline{c}_a$	root-mean-square chord of aileron behind hinge axis
V	true airspeed
V_i	indicated airspeed
p	local static pressure; also, rolling velocity when used in parameter pb/2V
H_o	free-stream total pressure
S	airfoil pressure coefficient $\frac{H_o - p}{q_o}$
pb/2V	helix angle described by wing tip during roll, radians
F_w	wheel force
θ	wheel deflection from neutral
C_{l_δ}	rate of change of rolling-moment coefficient with aileron deflection
C_{l_p}	rate of change of rolling-moment coefficient with pb/2V
c_l	airfoil section lift coefficient
Δc_l	increment of c_l caused by deflection of control surface from neutral
c_d	airfoil section drag coefficient

h control-surface hinge moment per unit span; positive when control surface tends to deflect downward

c_{h_x} control-surface section hinge-moment coefficient based on control-surface chord $\left(\frac{h}{q_o c_x^2}\right)$

$(c_{h_a})_{up}$ hinge-moment coefficient of upgoing aileron estimated for airplane during roll

$(c_{h_a})_{down}$ hinge-moment coefficient of downgoing aileron estimated for airplane during roll

$\Delta p/q_o$ seal-pressure-difference coefficient (ratio of pressure difference across control-surface seal to free-stream dynamic pressure); positive when pressure below seal is greater than pressure above seal

$\left(\frac{\partial c_l}{\partial \alpha_o}\right)_{\delta_x}$ rate of change of section lift coefficient with section angle of attack

$\left(\frac{\partial c_l}{\partial \delta_x}\right)_{\alpha_o}$ rate of change of section lift coefficient with control-surface deflection

$\left(\frac{\partial \alpha_o}{\partial \delta_x}\right)_{c_l}$ control-surface section effectiveness parameter (absolute value); also designated as k for aileron

$\left(\frac{\Delta \alpha_o}{\Delta \delta_a}\right)_{c_l}$ aileron section effectiveness parameter (ratio of increment of airfoil section angle of attack to increment of aileron deflection required to maintain a constant lift coefficient; absolute value)

$\left(\frac{\partial c_{h_x}}{\partial \alpha_o}\right)_{\delta_x}$ rate of change of section hinge-moment coefficient with section angle of attack

$\left(\frac{\partial c_{h_x}}{\partial \delta_x}\right)_{\alpha_o}$ rate of change of section hinge-moment coefficient with control-surface deflection

The subscript x is replaced herein with subscripts r, e, and a for the rudder, elevator, and aileron, respectively. The subscripts to the partial derivatives denote the variables held constant when the partial derivatives are taken. The derivatives are obtained at zero angle of attack and zero control-surface deflection except as noted.

MODELS AND APPARATUS

The three models, having chords of 24 inches, were two-dimensional airfoil sections designed for use as a vertical tail, a horizontal tail, and a wing and were constructed of laminated mahogany. Sketches of the models are presented as figure 1. Rubber seals were used along the complete span and at both ends of the control surfaces to prevent the flow of air through the gaps.

The pressure difference across the control-surface seals was measured with static-pressure orifices located above and below the balance plates. A manometer setup, which integrated the pressures along the floor and ceiling of the tunnel test section, was used to measure lift, and the wake survey method was used to measure drag. Hinge moments of the control surfaces were measured with electrical-resistance strain gages.

The vertical-tail section was a 0.155c thick symmetrical airfoil with a pressure distribution (fig. 2) similar to that of the NACA 64-series airfoils. The model was equipped with a 0.40c rudder with a sealed internal balance of $0.412c_r$, that is, $\frac{c_b}{c_r} = 0.412$.

The horizontal-tail section, which also had a pressure distribution (fig.3) similar to that of the NACA 64-series airfoils, had a maximum thickness of approximately 0.13c. The angle of attack for this model was measured with respect to a reference line shown in figure 1. The model was equipped with a 0.35c elevator with a sealed internal balance of approximately $0.43c_e$.

The wing profile had a maximum thickness of approximately 0.17c and a pressure distribution (fig. 4) similar to that of an NACA 7-series airfoil. The design section lift coefficient is 0.266, for which the position of

minimum pressure is approximately 0.35c on the upper surface and 0.50c on the lower surface. The airfoil section angle of attack was measured with respect to a reference line shown in figure 1. The model was equipped with a 0.22c aileron of true airfoil contour with a sealed internal balance of approximately $0.44c_a$.

For the normal smooth condition of the models, the airfoil surfaces were sanded with No. 400 carborundum paper to produce an aerodynamically smooth finish. For the rough condition of the vertical-tail section, the model surfaces were the same as for the smooth condition but 0.002-inch carborundum grains were applied to a thin layer of shellac on both the upper and lower airfoil surfaces at various chordwise positions. The roughness strips were 1.2 inches wide at 0.45c, 0.5 inch wide at 0.30c, 0.15c, and 0.10c, and 3.75 inches wide at the leading edge (1.875 in. along each surface measured from the leading edge).

TESTS

Tests of the three models were made in the Langley two-dimensional low-turbulence pressure tunnel. The tests included measurements at a Reynolds number of approximately 6×10^6 of airfoil lift and drag, control-surface hinge moment, and balance pressure for each model with various deflections of the control surfaces. Observations of the air flow over the surfaces of both tail sections were made by means of tuft surveys. Lift and drag measurements were also made at Reynolds numbers of approximately 3×10^6 and 9×10^6 for the horizontal- and vertical-tail sections with the control surfaces neutral. In addition, the vertical-tail section was tested at a Reynolds number of 6×10^6 with roughness strips applied to both upper and lower airfoil surfaces at various chordwise positions. The Mach numbers corresponding to Reynolds numbers of 3×10^6, 6×10^6, and 9×10^6 were 0.11, 0.14, and 0.10, respectively.

The following formulas were used to correct the tunnel data to free-air conditions:

$$c_l = \left[1 - 2\Lambda(\sigma + \xi) - \sigma\right] c_l'$$

$$c_d = \left[1 - 2\Lambda(\sigma + \xi)\right] c_d'$$

$$\alpha_o = (1 + \sigma)\alpha_o'$$

$$q_o = \left[1 + 2\Lambda(\sigma + \xi)\right] q_o'$$

where

Λ factor dependent on airfoil shape

σ factor dependent on ratio of airfoil size to tunnel height

ξ factor used for correcting effect of model upon velocity measured by static-pressure orifices

and the primed quantities represent the values measured in the tunnel.

The values of $2\Lambda(\sigma + \xi)$ were 0.0115, 0.00979, and 0.00792 for the wing, vertical-tail, and horizontal-tail sections, respectively. The value of σ was equal to 0.015 for all three airfoils.

RESULTS AND DISCUSSION

Values of the important aerodynamic parameters measured when α_o and δ_x are approximately 0 for the three models tested are presented in the following table:

Airfoil section	Airfoil surface condition	$\left(\frac{\partial c_l}{\partial \alpha_o}\right)_{\delta_x}$	$\left(\frac{\partial \alpha_o}{\partial \delta_x}\right)_{c_l}$	$\left(\frac{\partial c_{h_x}}{\partial \alpha_o}\right)_{\delta_x}$	$\left(\frac{\partial c_{h_x}}{\partial \delta_x}\right)_{\alpha_o}$
Rudder	Smooth	0.107	0.58	-0.0034	-0.0007
	L.E. rough	.107	.58	-.0009	-------
Elevator	Smooth	.100	.62	-.0029	-.0023
Aileron	Smooth	.101	.48	-.0004	-.0013

Vertical-Tail Section

Lift, hinge-moment, balance-pressure, and drag data for the vertical-tail section with the airfoil surfaces aerodynamically smooth and also with roughness strips applied at various chordwise positions are presented in figures 5 to 14.

Lift.- The lift characteristics of the vertical-tail section at a Reynolds number of approximately 6×10^6 are presented in figure 5 for the airfoil in a smooth condition. The values of $\left(\frac{\partial c_l}{\partial \alpha_o}\right)_{\delta_r}$ and $\left(\frac{\partial c_l}{\partial \delta_r}\right)_{\alpha_o}$ are equal to 0.107 and 0.062, respectively, and the effectiveness parameter $\left(\frac{\partial \alpha_o}{\partial \epsilon_r}\right)_{c_l}$ is equal to 0.58. The increment of section lift coefficient Δc_l plotted against rudder deflection is presented in figure 6 for four section angles of attack from 0° to 12°. These curves show that for small rudder deflections the effectiveness remains constant through this range of angle of attack. At rudder deflections more negative than -2°, the increment of section lift coefficient increases with decreasing angle of attack until the air flow over the lower surface of the rudder begins to separate. This separation occurs at low angles of attack for high negative rudder deflections as shown in figures 5 and 6 and was observed by means of tuft surveys over the airfoil surfaces.

Scale effect on the lift characteristics is shown in figure 7. Lift measurements were made with the rudder neutral at Reynolds numbers of approximately 3×10^6, 6×10^6, and 9×10^6.

The effect of fixed transition on the lift characteristics at rudder deflections of 0°, -5°, and -10° is shown in figure 8. Application of roughness to the airfoil leading edge caused an average reduction in maximum section lift coefficient of approximately 12 percent but had a negligible effect on the lift-curve slope with the rudder neutral. The values of $\left(\frac{\partial c_l}{\partial \delta_r}\right)_{\alpha_o}$

and $\left(\frac{\partial \alpha_o}{\partial \delta_r}\right)_{c_l}$ that were obtained between rudder deflections of -5° and 0° and at zero angle of attack remained the same as for the aerodynamically smooth condition, but the increment of c_l caused by rudder deflections of -5° and -10° decreased at low angles of attack when transition was induced at the airfoil leading edge (fig. 8); the sharp irregularity in the variation of Δc_l with δ_r shown in figure 6 was thereby eliminated.

Hinge moment.- The variation of rudder section hinge-moment coefficient c_{h_r} with airfoil section angle of attack for the smooth airfoil is presented in figure 9 for rudder deflections between -19° and 19° at a Reynolds number of approximately 6×10^6. Corresponding curves of the pressure difference across the rudder balance seal $\Delta p/q_o$ against α_o are presented in figure 11. These data may be used to estimate the hinge-moment characteristics of a rudder of similar contour and chord by the methods of reference 1. For the 41.2-percent sealed internal balance, the values of $\left(\frac{\partial c_{h_r}}{\partial \alpha_o}\right)_{\delta_r}$ and $\left(\frac{\partial c_{h_r}}{\partial \delta_r}\right)_{\alpha_o}$ were equal to -0.0034 and -0.0007, respectively, for the airfoil surfaces in a smooth condition.

The sharp irregularities in the curves of c_{h_r} against α_o (fig. 9) correspond to the limits of the low-drag range as shown in figure 13 and are believed to be caused by the sudden movements in transition along the airfoil surfaces at the extremities of the low-drag range. The data of figure 10 were taken at rudder deflections of 0°, -5°, and -10° with transition strips placed on the airfoil surfaces at various chordwise positions to limit the movement of transition. As the fixed transition was moved forward of the 0.15c position the irregularities in $\left(\frac{\partial c_{h_r}}{\partial \alpha_o}\right)_{\delta_r}$ diminished in magnitude but were not entirely removed until transition was fixed

at the airfoil leading edge. The value of $\left(\frac{\partial c_{h_r}}{\partial \alpha_o}\right)_{\delta_r}$ with transition fixed at the airfoil leading edge was -0.0009 as compared with -0.0034 for the aerodynamically smooth airfoil. A forward position of transition had no significant effect on the variation of $\Delta p/q_o$ with α_o (fig. 12).

Drag.- Drag characteristics of the vertical-tail section in a smooth condition are presented in figure 13 at Reynolds number of approximately 3×10^6, 6×10^6, and 9×10^6 with the rudder neutral and at a Reynolds number of approximately 6×10^6 with rudder deflections between -5° and 5°. Through this range of rudder deflection the value of the minimum section drag coefficient and the range of lift coefficient for low-drag values remained substantially the same. Drag polars for the airfoil section with transition strips applied to the airfoil surfaces at various chordwise positions are presented in figure 14 for rudder deflections of 0° and -5°.

Horizontal-Tail Section

Lift, hinge-moment, balance-pressure, and drag data for the horizontal-tail section with the airfoil surfaces aerodynamically smooth are presented in figures 15 to 20.

Lift.- The lift characteristics of the horizontal-tail section at a Reynolds number of approximately 6×10^6 are presented in figure 15 for various elevator deflections between -23° and 9°. The values of $\left(\frac{\partial c_l}{\partial \alpha_o}\right)_{\delta_e}$ and $\left(\frac{\partial c_l}{\partial \delta_e}\right)_{\alpha_o}$ are equal to 0.100 and 0.062, respectively, and the effectiveness parameter $\left(\frac{\partial \alpha_o}{\partial \delta_e}\right)_{c_l}$ is equal to 0.62. The variation of the increment of section lift coefficient Δc_l with elevator deflection is presented in figure 16 for four section angles of attack from -4° to 8°. Between elevator deflections of -3° and 3° the effectiveness remains constant throughout this range of angle of attack. At elevator deflections more negative than -3° the increment of section

lift coefficient increases with decreasing section angle of attack until, as in the case of the rudder, the air flow over the lower surface of the elevator begins to separate. This separation, which was observed by means of tuft surveys over the airfoil surfaces, causes the sharp breaks in the lift curves of figure 15 and results in the decreased value of Δc_l at high negative elevator angles and low angles of attack (fig. 16). At positive elevator deflections greater than 4°, the value of Δc_l decreases with increasing angle of attack.

The effect of Reynolds number between 3×10^6 and 9×10^6 on the lift characteristics of the horizontal-tail section with the elevator neutral is shown in figure 17.

Hinge moment.- The elevator section hinge-moment coefficients plotted against airfoil section angle of attack are presented in figure 18 for elevator deflections between -23° and 9° at a Reynolds number of approximately 6×10^6. As in the case of the rudder tests, irregularities in the variation of c_{h_e} with α_o correspond to the limits of the low-drag range as shown in figure 20 and are believed to be caused by the sudden movements in transition along the airfoil surfaces at the extremities of the low-drag range. The value of $\left(\frac{\partial c_{h_e}}{\partial \alpha_o}\right)_{\delta_e}$ is equal to -0.0029 and was obtained at an angle of attack of -2° because one of the jogs in the hinge-moment curve occurs at a section angle of attack of 0°. If transition occurs on the airfoil surfaces at a forward chordwise position because of surface irregularities or roughness, the magnitude of the jogs in the curve of the variation of hinge moment with angle of attack and the absolute value of $\left(\frac{\partial c_{h_e}}{\partial \alpha_o}\right)_{\delta_e}$ may be expected to decrease in a manner similar to that of the vertical-tail section. The value of $\left(\frac{\partial c_{h_e}}{\partial \delta_e}\right)_{\alpha_o}$ for the aerodynamically smooth horizontal-tail section is approximately -0.0023.

The variation of the pressure difference across the elevator balance seal with α_o is presented in figure 19 at the same elevator deflections for which hinge-moment data are presented. The hinge-moment and seal-pressure data may be used to estimate the hinge-moment characteristics of an elevator of similar contour and chord with any amount of sealed internal balance by the methods of reference 1.

Drag.- Drag characteristics of the horizontal-tail section are presented in figure 20. These data include drag polars at Reynolds number of approximately 3×10^6, 6×10^6, and 9×10^6 with the elevator neutral and at a Reynolds number of 6×10^6 with the elevator deflected $\pm 2^\circ$.

Wing Section

Lift, hinge-moment, balance-pressure, and drag data for the wing section with the airfoil surfaces aerodynamically smooth are presented in figures 21 to 25.

Lift.- The lift characteristics of the airfoil section with an aileron are presented in figure 21. The values of $\left(\frac{\partial c_l}{\partial \alpha_o}\right)_{\delta_a}$ and $\left(\frac{\partial c_l}{\partial \delta_a}\right)_{\alpha_o}$ are equal to 0.101 and 0.048, respectively. The effectiveness parameter $\left(\frac{\partial \alpha_o}{\partial \delta_a}\right)_{c_l}$ is equal to 0.48 or 84 percent of the thin airfoil theoretical effectiveness (reference 2) and is approximately the same as the effectiveness obtained on the NACA 0009 airfoil section (reference 3).

In order to show the variation of aileron effectiveness with lift coefficient and aileron deflection, values of the effectiveness have been measured between definite aileron deflections. This effectiveness parameter is designated $\left(\frac{\Delta \alpha_o}{\Delta \delta_a}\right)_{c_l}$. Curves of $\left(\frac{\Delta \alpha_o}{\Delta \delta_a}\right)_{c_l}$ against c_l for various aileron deflection limits are presented in

figure 22. A comparison of the measured effectiveness between $\delta_a = 0^\circ$ and 10° and $\delta_a = 0^\circ$ and -10° shows that the aileron is more effective for negative aileron deflections. A comparison of the measured effectiveness between $\delta_a = 0^\circ$ and 17° and $\delta_a = 0^\circ$ and -17° also shows a higher effectiveness for negative aileron deflections except through an approximate range of section lift coefficient from 0 to 0.3 in which the effectiveness of the down aileron was about the same as that of the up aileron. At the section lift coefficients greater than approximately 0.4 the effectiveness of the aileron deflected down 17° decreased appreciably. This large decrease in effectiveness at high positive aileron deflections and section angles of attack, probably caused by separation of the air flow over the upper surface of the aileron, is reflected in a decrease in the effectiveness from $\delta_a = \pm 10^\circ$ to $\delta_a = \pm 17^\circ$. At section lift coefficients from -0.4 to 0.4 the effectiveness between the limits of $\delta_a = \pm 17^\circ$ was almost the same as that measured between the limits of $\delta_a = \pm 10^\circ$. The value of $\left(\frac{\Delta \alpha_o}{\Delta \delta_a}\right)_{c_l}$ when measured between $\delta_a = \pm 10^\circ$ decreased from 0.50 at a section lift coefficient of 0 to 0.48 at a section lift coefficient of 0.70 or only 4 percent and, when measured between $\delta_a = 17^\circ$ and $\delta_a = -17^\circ$ decreased from 0.50 to 0.45 or 10 percent over the same lift-coefficient range.

Hinge moment.- The variations of aileron section hinge-moment coefficient c_{h_a} with section angle of attack α_o for all aileron deflections tested are presented in figure 23(a). The irregularities in $\left(\frac{\partial c_{h_a}}{\partial \alpha_o}\right)_{\delta_a}$ shown by these curves are probably caused by the sudden movements in transition on the upper and lower airfoil surfaces at the extremities of the low-drag range. (See fig. 25.) No sharp irregularities are apparent, however, in the

variation of c_{h_a} with aileron deflection as shown by the curves of figure 23(b). The values of $\left(\frac{\partial c_{h_a}}{\partial \alpha_o}\right)_{\delta_a}$ and $\left(\frac{\partial c_{h_a}}{\partial \delta_a}\right)_{\alpha_o}$ are 0.0004 and -0.0013, respectively, for the aerodynamically smooth airfoil.

The variation of the pressure difference across the aileron balance seal $\Delta p/q_o$ with α_o is presented in figure 24 for all aileron deflections tested. The basic data of figures 23(a) and 24 may be used to estimate the section characteristics of an aileron of similar contour and chord with any amount of sealed internal balance by the methods of reference 1.

Drag.- The variation of section drag coefficient with section lift coefficient at a Reynolds number of approximately 6×10^6 for aileron deflections of 0°, 5°, and -5° is presented in figure 25. The minimum section drag coefficient was approximately the same for the three aileron deflections, although the extent of the low-drag range was reduced with the aileron deflected ±5° to about one-half the range with the aileron neutral.

Effects of Sudden Movement of Transition on Airplane Control-Surface Characteristics

The two-dimensional data presented herein show sudden changes in the variation of control-surface section hinge-moment coefficient with airfoil section angle of attack when transition suddenly moves forward along the airfoil surfaces. The effect of sudden movements of transition on the airplane control forces was investigated. In order to determine whether the irregularities in the two-dimensional hinge-moment characteristics would cause unusual aileron wheel-force characteristics, the variation of wheel force F_w with wing-tip helix angle pb/2V for an assumed airplane was estimated for various indicated airspeeds (fig. 26). The values of pb/2V were estimated from the following equation presented in reference 4:

$$\frac{pb}{2V} = \frac{C_{l_\delta}\, k\, \Delta\delta_a}{k\, 114.6\, C_{l_p}} \qquad (1)$$

Test values of $\Delta\alpha_o$ were substituted in equation (1) for the product $k\,\Delta\delta_a$, and values of $\frac{C_{l_\delta}}{k}$ and C_{l_p} equal to 0.331 and 0.495, respectively, were obtained from reference 4 by use of the following assumed airplane dimensions:

Wing span, feet	70.5
Wing area, square feet	554
Wing loading, pounds per square foot	45
Aspect ratio	9
Taper ratio	3
Aileron span, feet	11.5
Aileron root-mean-square chord behind hinge axis, feet	1.8
Aileron location, fraction of semispan	
Inboard end	0.668
Outboard end	1.000
Wheel diameter, feet	1.083
Maximum wheel deflection, degrees	±175

Wheel forces were estimated from the equation

$$F_w = \frac{q_o b_a \bar{e}_a^2}{\text{Wheel radius}} \left[\left(\frac{d\delta_a}{d\theta} \right)_{up} \left(c_{h_a} \right)_{up} - \left(\frac{d\delta_a}{d\theta} \right)_{down} \left(c_{h_a} \right)_{down} \right] \qquad (2)$$

The aileron hinge-moment coefficients $\left(c_{h_a}\right)_{up}$ and $\left(c_{h_a}\right)_{down}$ were estimated from the section data for the airplane in a steady roll. Values of these coefficients were taken at given aileron angles and corrected for the change in angle of attack at the aileron midspan caused by the roll. Equal up and down aileron deflections and a maximum wheel deflection of 175° were used.

Because the values of pb/2V were not corrected for wing twist, control-system stretch, or adverse yaw and the section hinge-moment coefficients were not corrected for

aspect-ratio effects, the estimated values of $pb/2V$ and F_w are not quantitatively accurate. The values are useful, however, to show the qualitative variation of wheel force with wing-tip helix angle.

No sudden changes in the estimated variation of F_w with $pb/2V$ are apparent in figure 26, which indicates that inclusion of the hinge moments due to the deflection of both ailerons tends to eliminate the irregularities in the hinge-moment variation with angle of attack alone. If the angle of attack were varied with the ailerons neutral, however, both the right and left ailerons would tend to move in the same direction when the change in angle of attack causes transition to move forward suddenly, and the effect would be absorbed in the aileron rigging with no change in the wheel force.

Data recently obtained in the Langley stability tunnel indicate that sudden movements of transition cause irregularities in the variation of hinge-moment coefficient with angle of attack in three-dimensional flow as well as in two-dimensional flow. Sudden movements of transition along the surfaces of vertical- or horizontal-tail sections, therefore, will probably cause sudden changes in rudder or elevator hinge moments. The data obtained with transition fixed at various locations along the airfoil surfaces, however, indicate a decrease in the severity of the jogs in the variation of c_{h_x} with α_o as the location of transition is moved toward the airfoil leading edge. Sudden changes in elevator and rudder forces, therefore, seem less likely to occur on an airplane since the full extent of laminar flow on production airplanes has not been realized because of manufacturing irregularities and surface deterioration in service and because transition is induced near or at the leading edge of tail surfaces that are located within the propeller slipstream or wing and fuselage wake.

CONCLUDING REMARKS

Results of a two-dimensional wind-tunnel investigation of a low-drag vertical-tail, horizontal-tail, and wing section equipped with sealed internally balanced control surfaces have been presented. Sharp irregularities occurred in the variation of the control-surface section

hinge-moment coefficient with section angle of attack, which were probably caused by sudden movements in transition along the surfaces of the airfoils at the extremities of the low-drag range. Tests of the vertical-tail section indicated that these irregularities were reduced in magnitude when transition was fixed at a forward chordwise position but were not entirely removed until transition was fixed at the airfoil leading edge. An estimated variation of aileron wheel force with wing-tip helix angle for an assumed airplane indicated that no unusual aileron wheel-force characteristics would be caused by the irregularities in the two-dimensional hinge-moment characteristics. Sudden changes in rudder or elevator hinge moments, however, would probably result from sudden movements in transition along the surfaces of the vertical- or horizontal-tail sections. If transition should occur at or near the leading edge of the tail surfaces, as is usually the case for tail surfaces located within the propeller slipstream or wing and fuselage wake, no sudden changes would occur in the control-surface hinge moments.

Langley Memorial Aeronautical Laboratory
National Advisory Committee For Aeronautics
Langley Field, Va., March 8, 1946

REFERENCES

1. Fischel, Jack: Hinge Moments of Sealed-Internal-Balance Arrangements for Control Surfaces. II - Experimental Investigation of Fabric Seals in the Presence of a Thin-Plate Overhang. NACA ARR No. L5F30a, 1945.

2. Glauert, H.: Theoretical Relationships for an Aerofoil with Hinged Flap. R. & M. No. 1095, British A.R.C., 1927.

3. Ames, Milton B., Jr., and Sears, Richard I.: Determination of Control-Surface Characteristics from NACA Plain-Flap and Tab Data. NACA Rep. No. 721, 1941.

4. Gilruth, R.R., and Turner, W.N.: Lateral Control Required for Satisfactory Flying Qualities Based on Flight Tests of Numerous Airplanes. NACA Rep. No. 715, 1941.

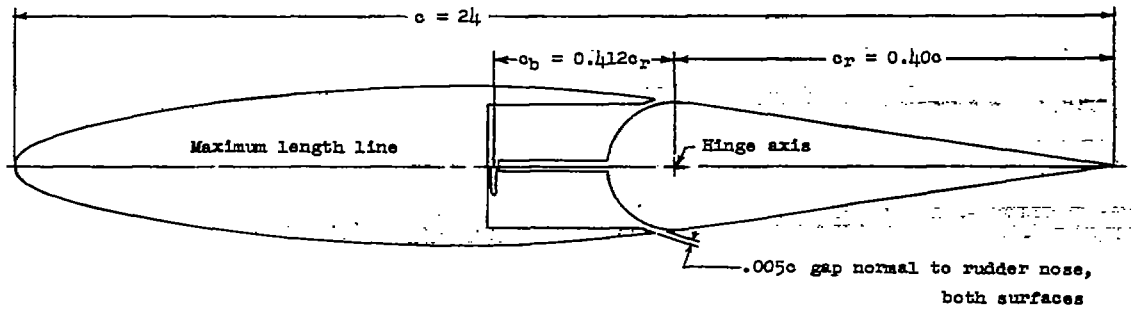

Vertical-tail section

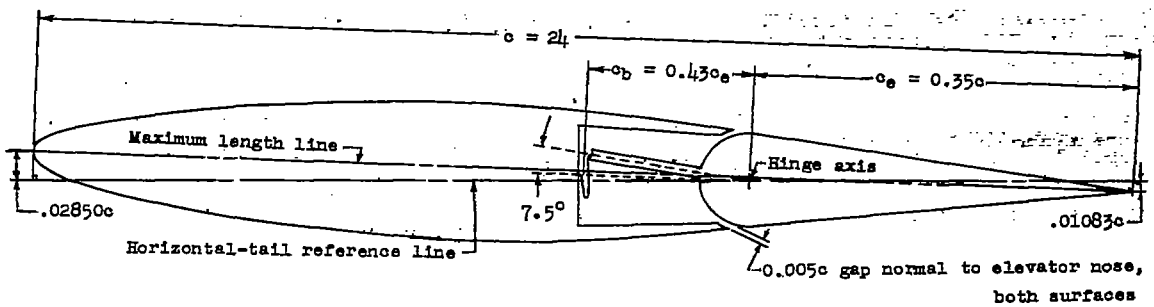

Horizontal-tail section

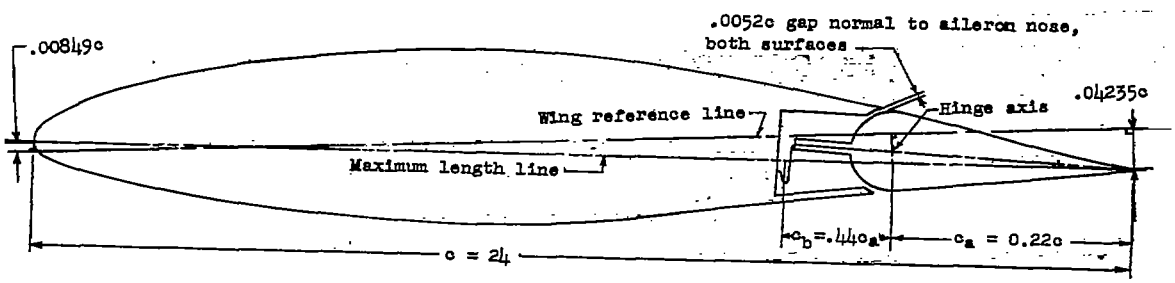

Wing section

NATIONAL ADVISORY COMMITTEE FOR AERONAUTICS.

Figure 1.- Vertical-tail, horizontal-tail, and wing sections.

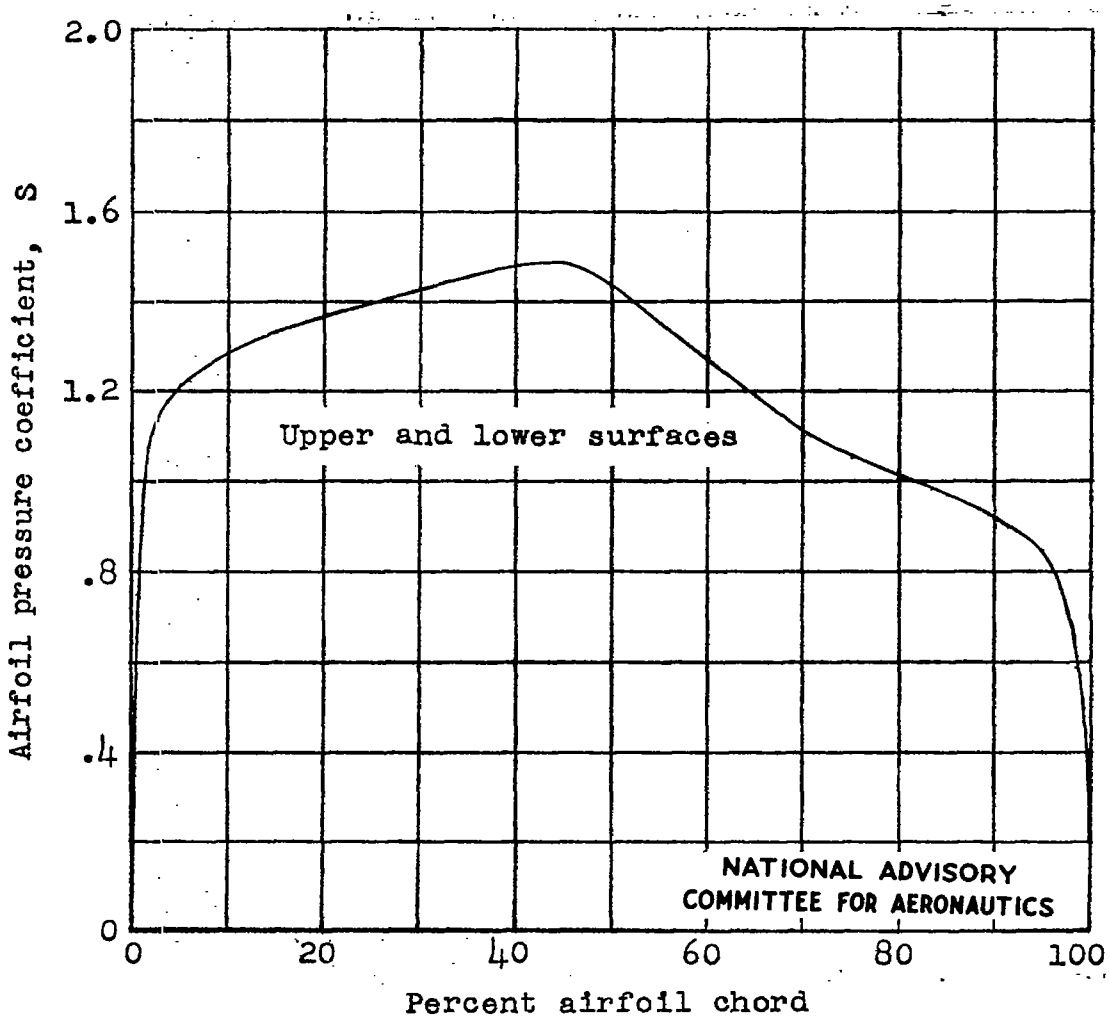

Figure 2.- Theoretical pressure distribution at zero lift of the low-drag vertical-tail section.

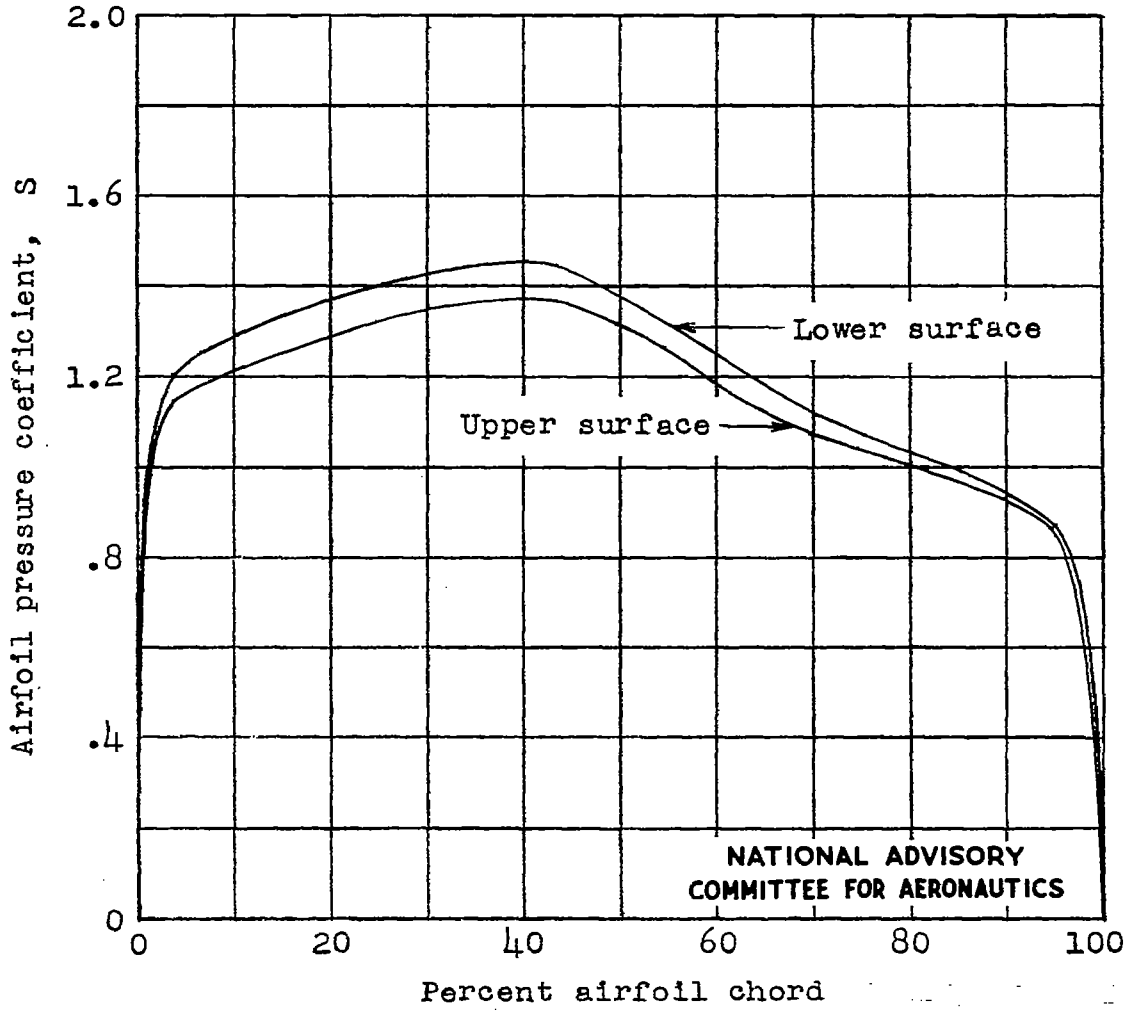

Figure 3.- Theoretical pressure distribution at a section lift coefficient of -0.053 of the low-drag horizontal-tail section.

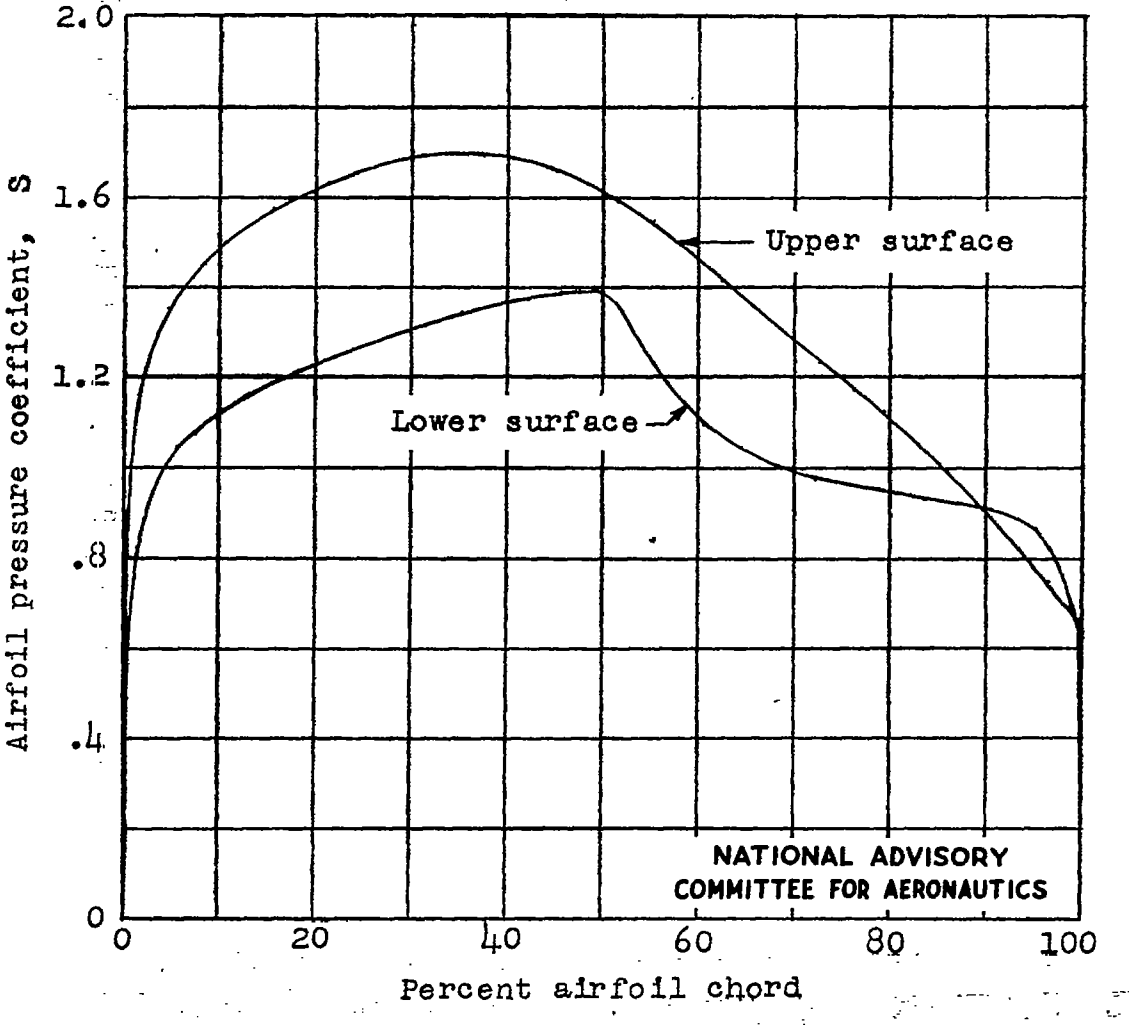

Figure 4.- Theoretical pressure distribution at a section lift coefficient of 0.266 of the low-drag wing section.

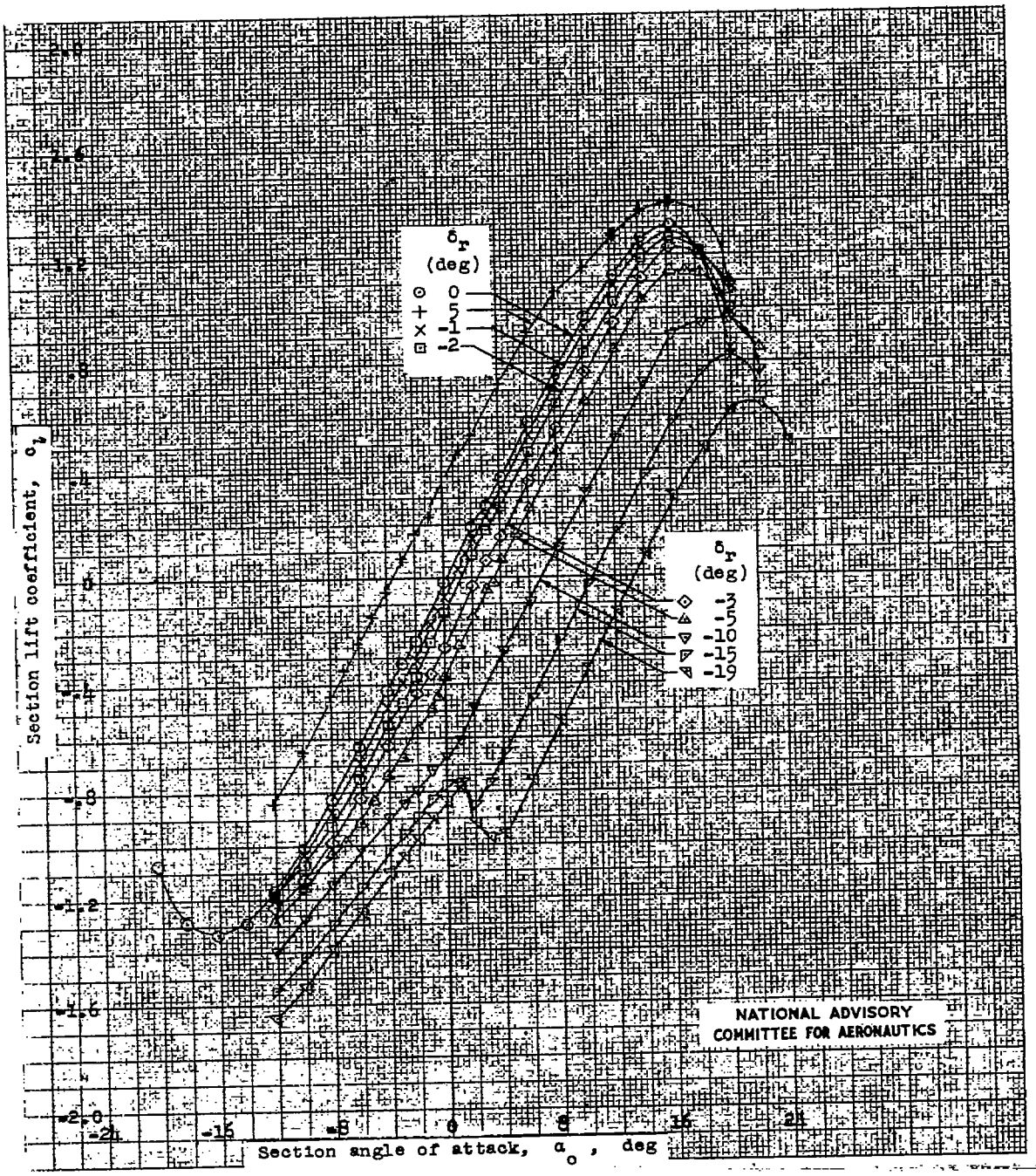

Figure 5.- Lift characteristics of a low-drag vertical-tail section equipped with a 0.40c sealed internally balanced rudder. Smooth condition; R = 6 × 10^6 (approx.); test, TDT 582.

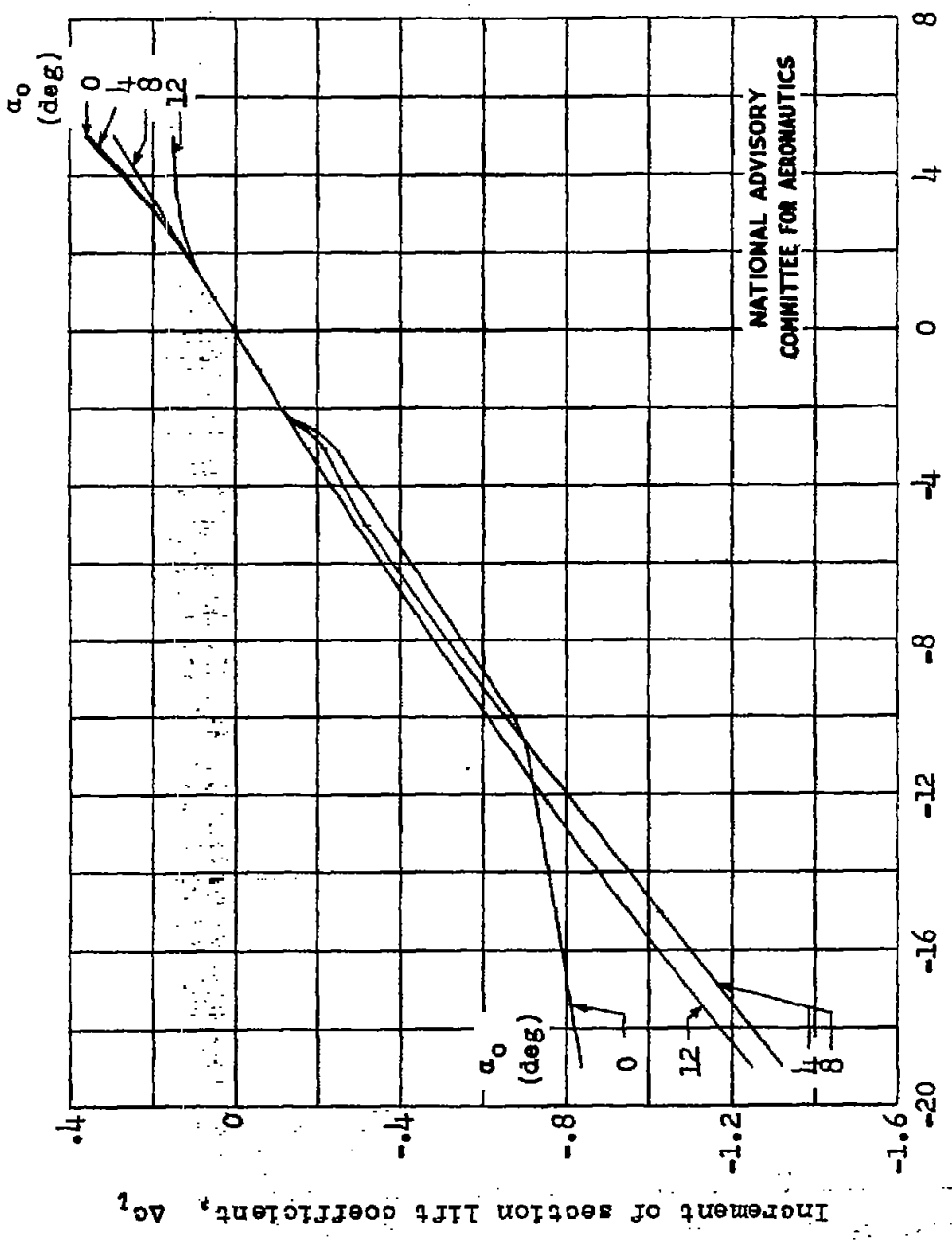

Figure 6.- Variation of Δc_l with δ_r at constant α_o for a low-drag vertical-tail section equipped with a 0.40c sealed internally balanced rudder. Smooth condition; $R = 6 \times 10^6$ (approx.).

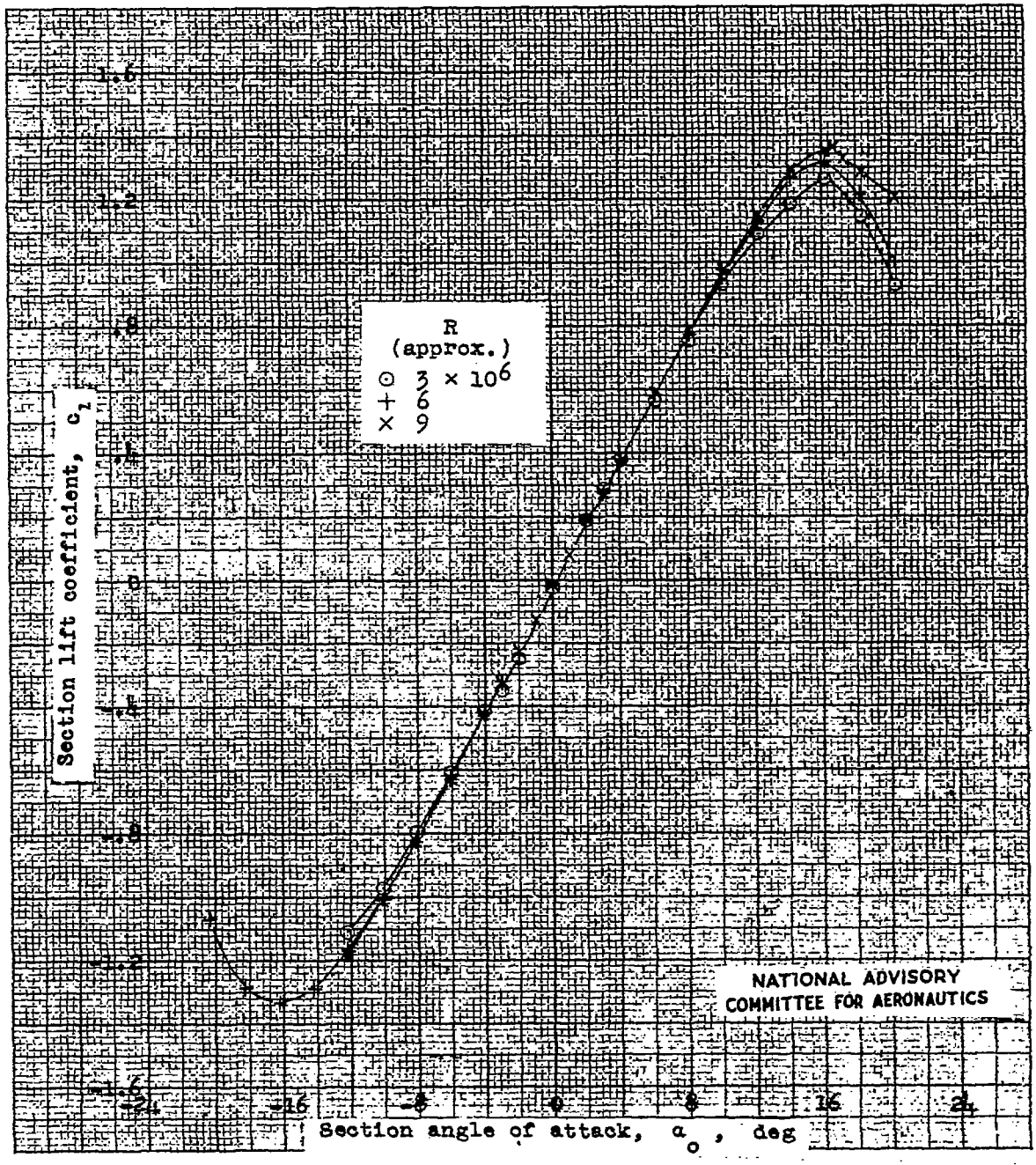

Figure 7.- Lift characteristics of a low-drag vertical-tail section equipped with a 0.40c sealed internally balanced rudder. Smooth condition; $\delta_r = 0^\circ$; test, TDT 582.

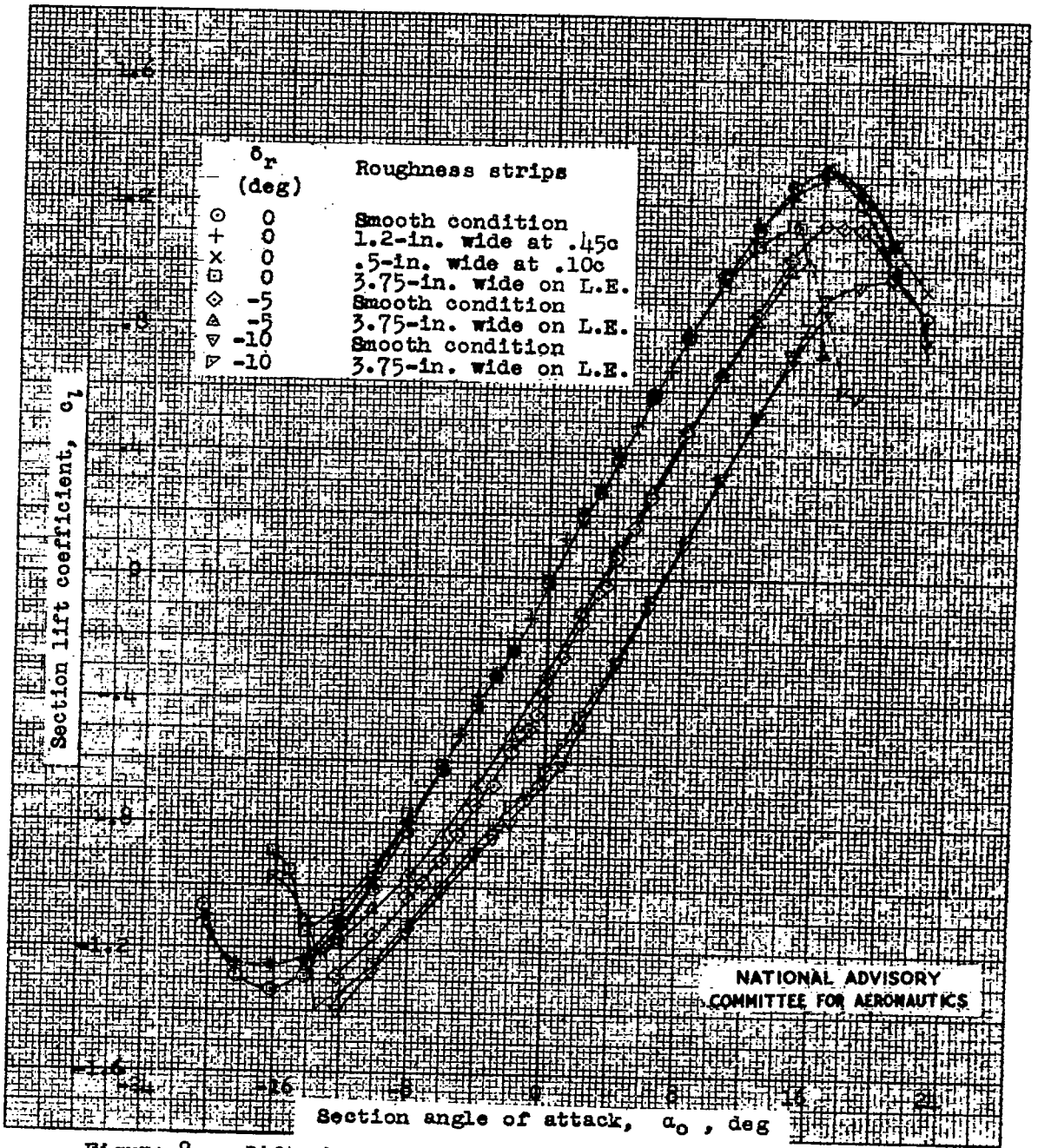

Figure 8.- Lift characteristics of a low-drag vertical-tail section equipped with a 0.40c sealed internally balanced rudder. Strips of 0.002-inch carborundum grains on both airfoil surfaces at various chordwise positions; $R = 6 \times 10^6$ (approx.); test, TDT 585.

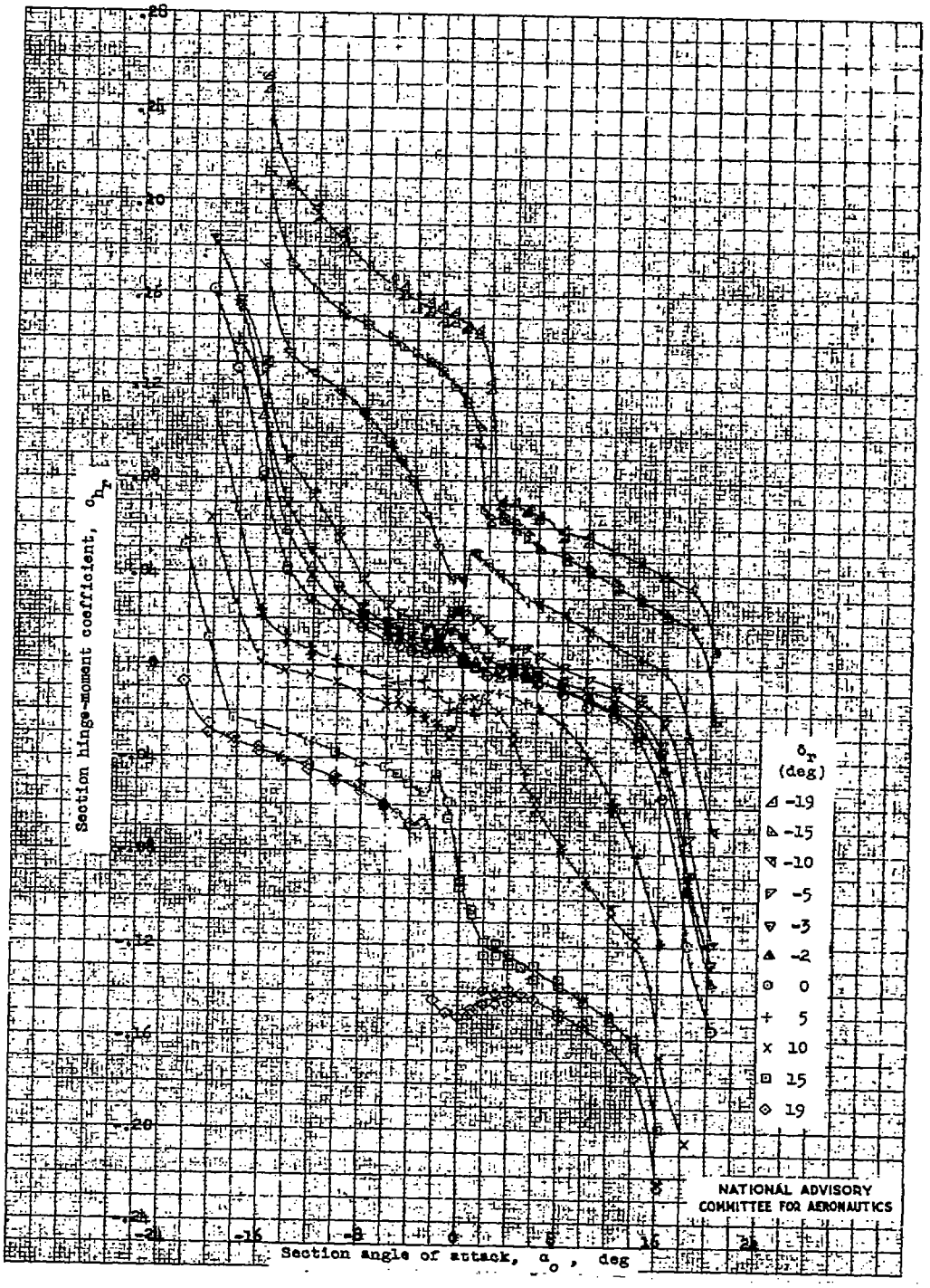

Figure 9.- Hinge-moment characteristics of a 0.40c sealed internally balanced rudder on a low-drag vertical-tail section. Smooth condition; R = 6×10^6 (approx.); test, TDT 584.

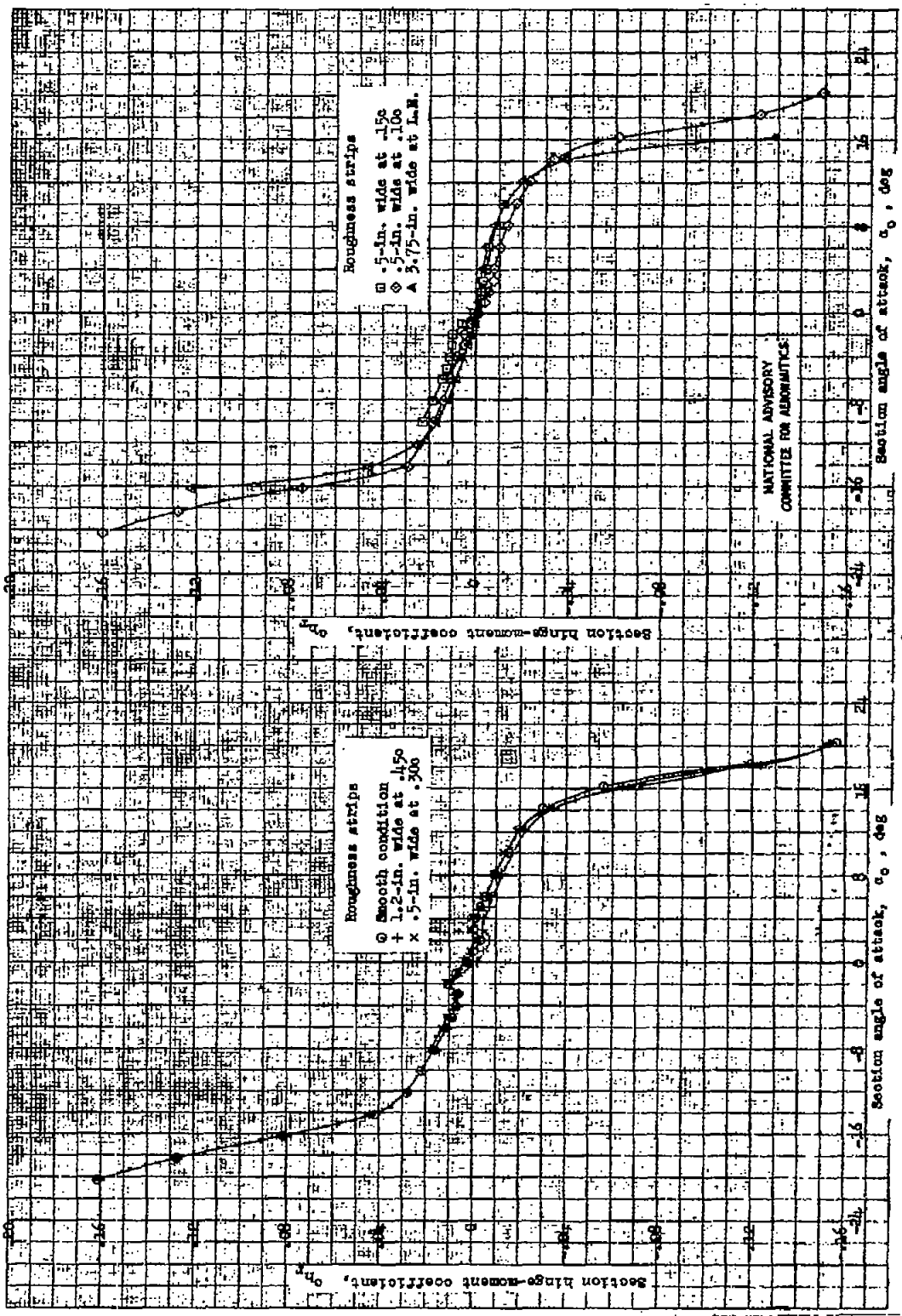

Figure 10.- Hinge-moment characteristics of a 0.40c sealed internally balanced rudder on a low-drag vertical-tail section. Strips of 0.002-inch carborundum grains on both airfoil surfaces at various chordwise positions; $R = 6 \times 10^6$ (approx.); test, MT 585.

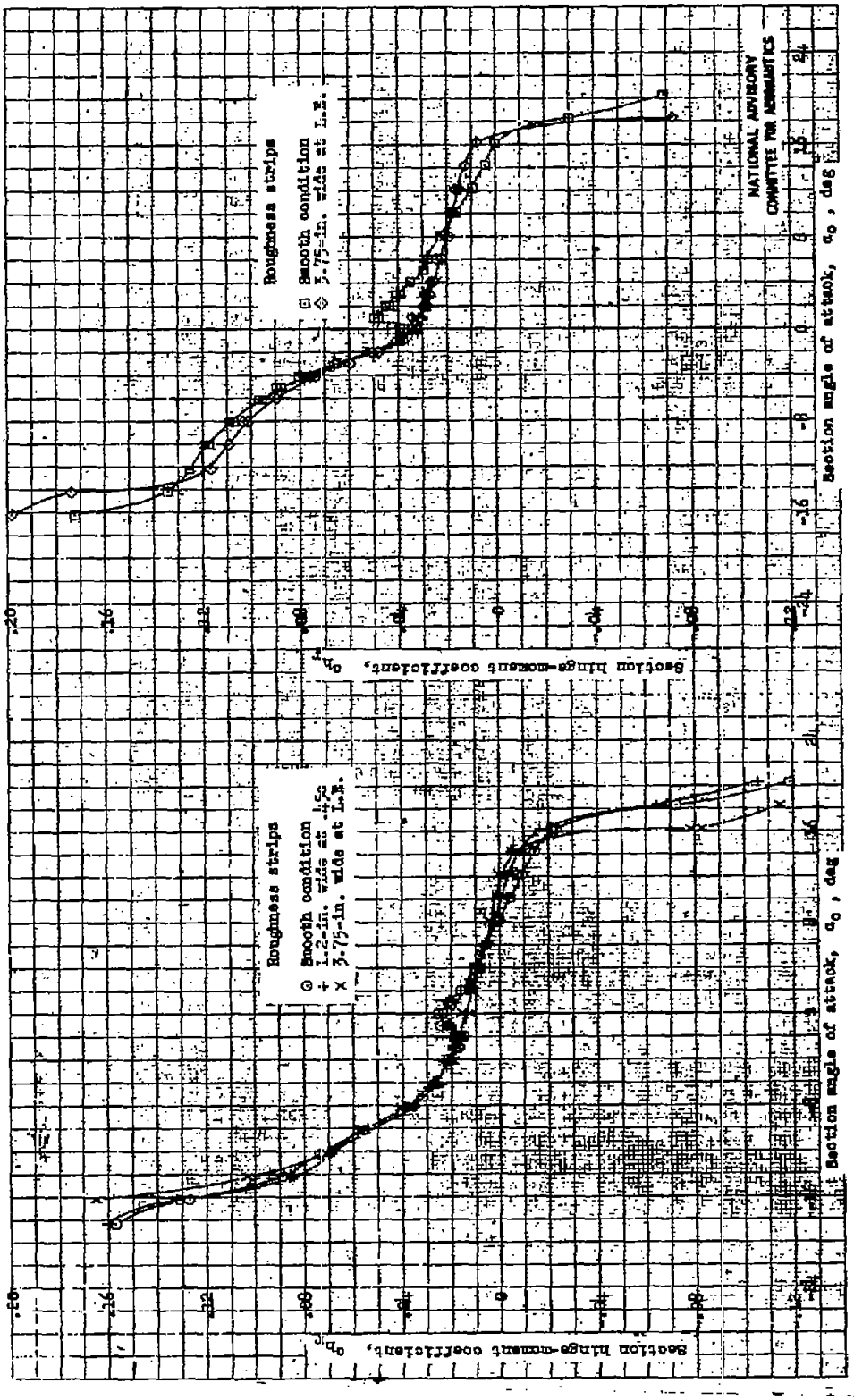

Figure 10.- Concluded.

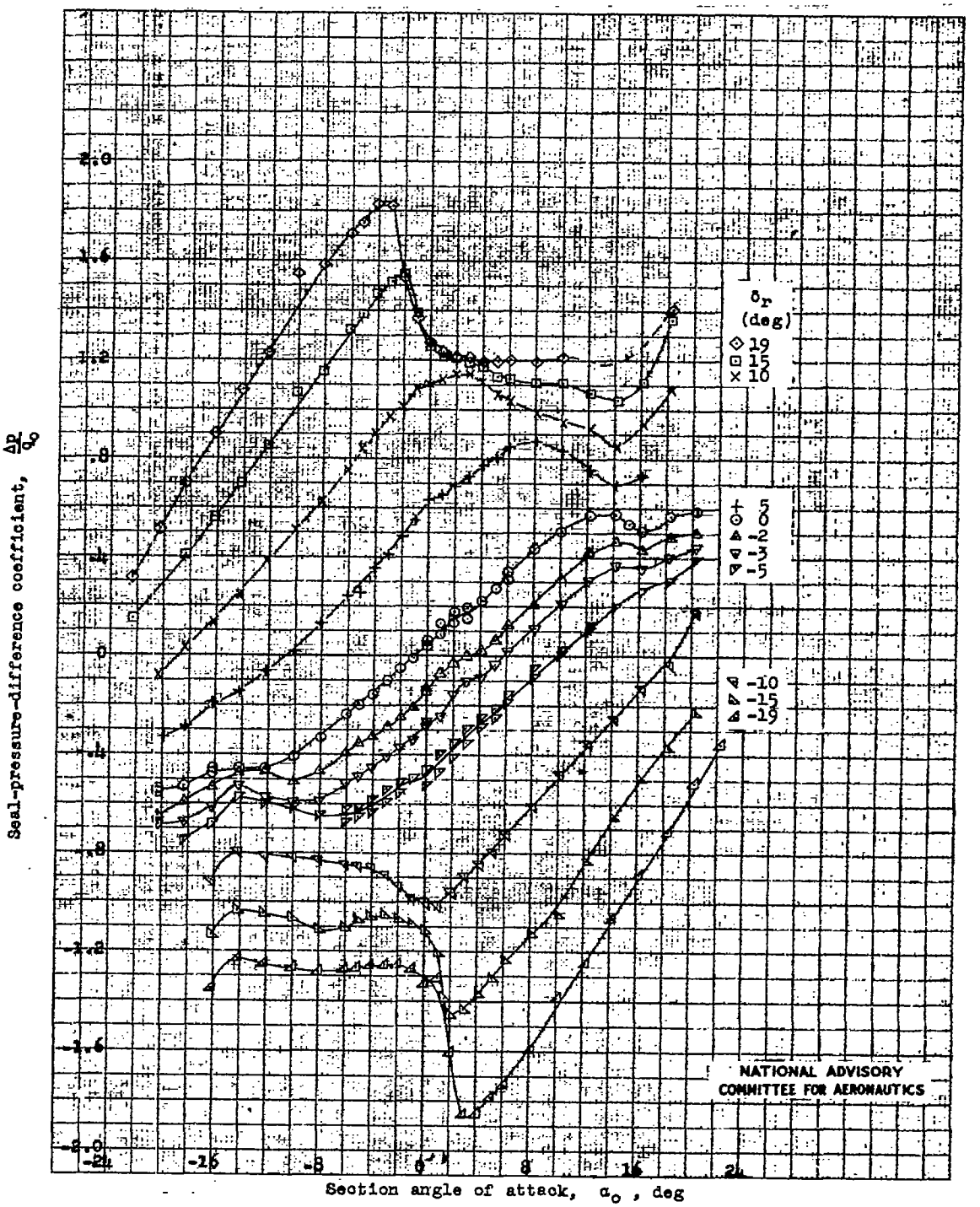

Figure 11.- Variation of $\frac{\Delta p}{q_o}$ with α_o for a 0.40c sealed internally balanced rudder on a low-drag vertical-tail section. Smooth condition; $R = 6 \times 10^6$ (approx.); test, TDT 584.

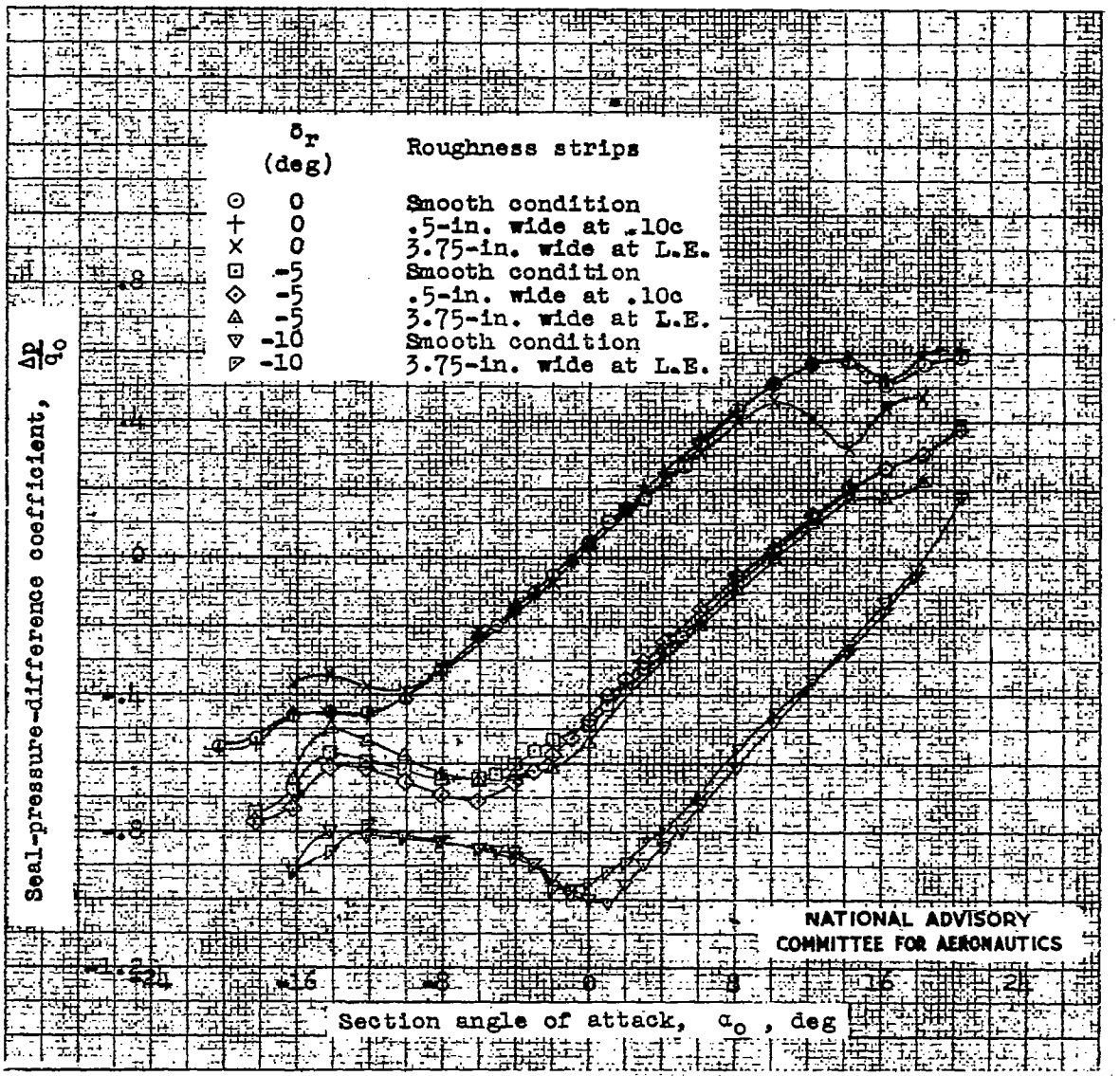

Figure 12.- Variation of $\frac{\Delta p}{q_o}$ with α_o for a 0.40c sealed internally balanced rudder on a low-drag vertical-tail section. Strips of 0.002-inch carborundum grains on both airfoil surfaces at various chordwise positions; R = 6×10^6 (approx.); test, TDT 585.

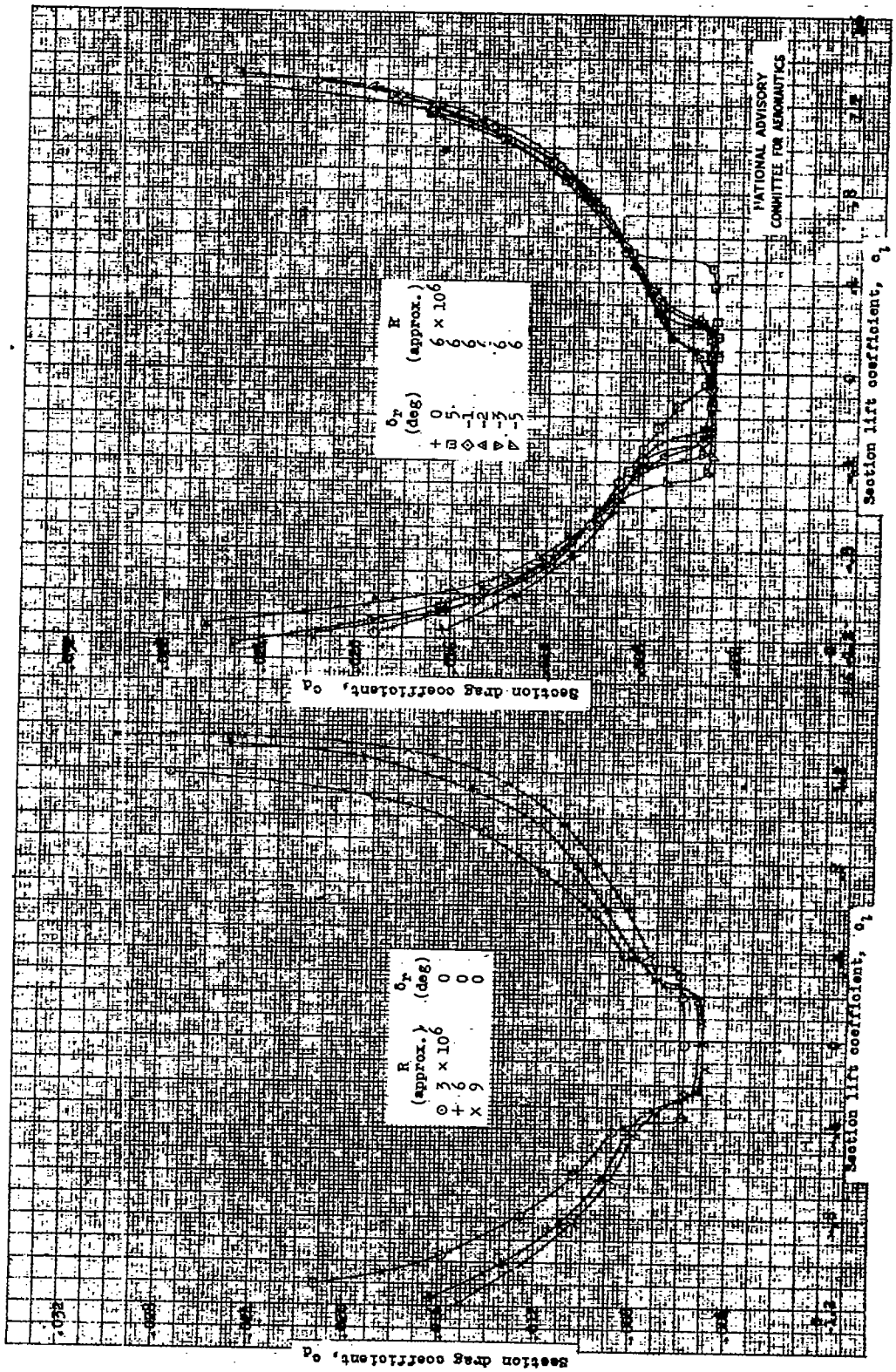

Figure 13.- Drag characteristics of a low-drag vertical-tail section equipped with a 0.40c sealed internally balanced rudder. Smooth condition; test EVT 542.

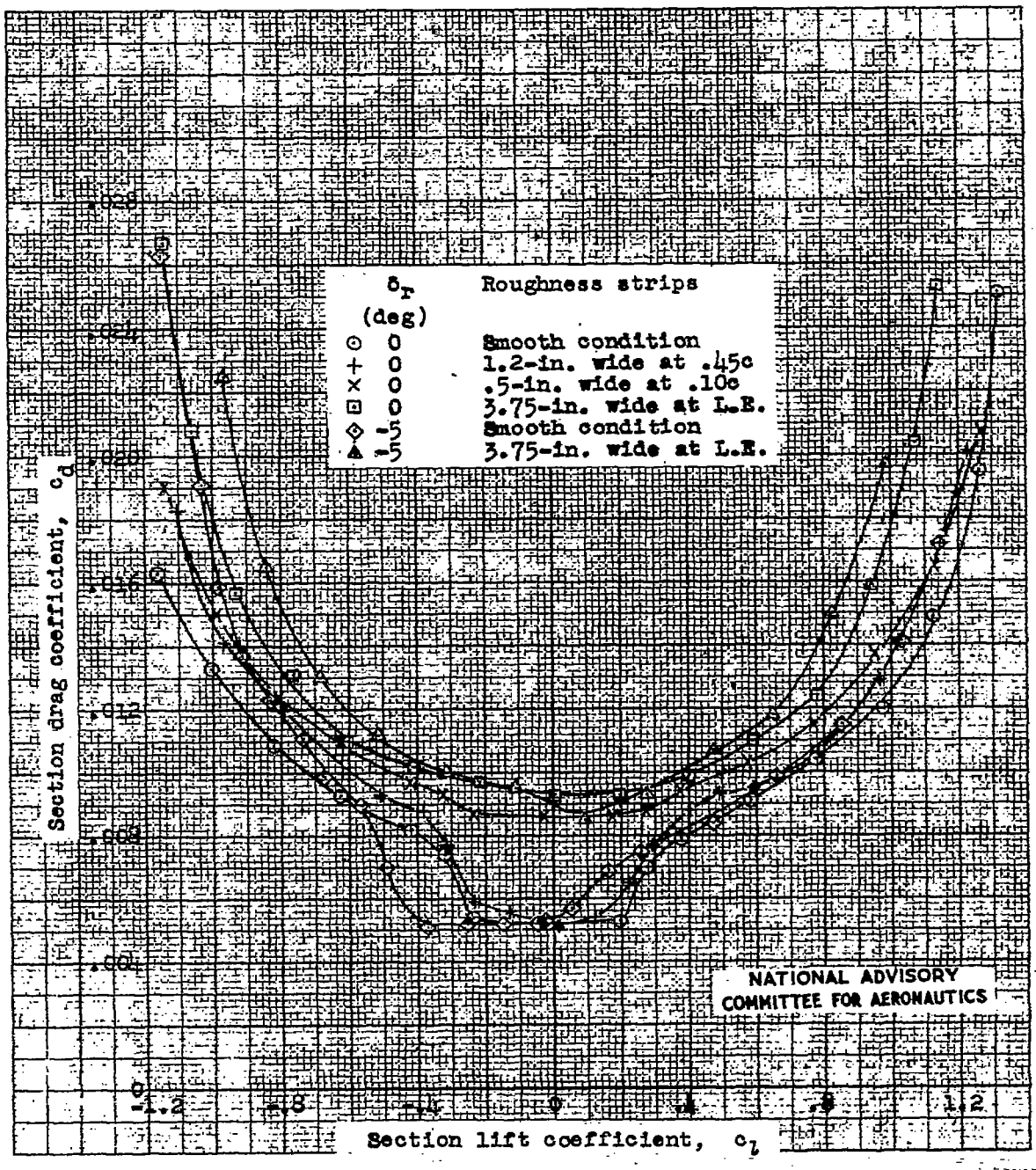

Figure 14.- Drag characteristics of a low-drag vertical-tail section equipped with a 0.40c sealed internally balanced rudder. Strips of 0.002-inch carborundum grains on both airfoil surfaces at various chordwise positions; $R = 6 \times 10^6$ (approx.); test, TDT 585.

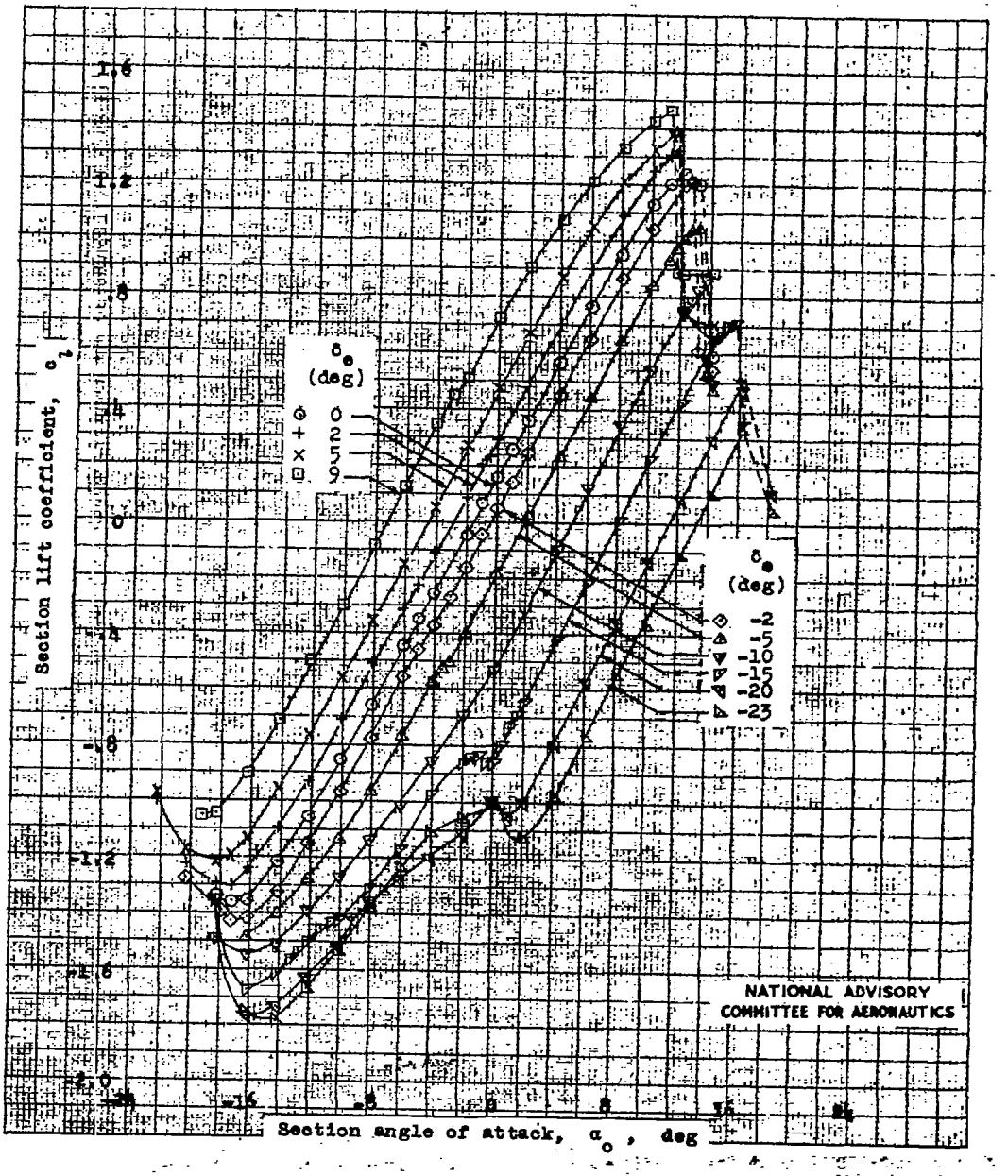

Figure 15.- Lift characteristics of a low-drag horizontal-tail section equipped with a 0.35c sealed internally balanced elevator. $R = 6 \times 10^6$ (approx.); tests, TDT 581 and 589.

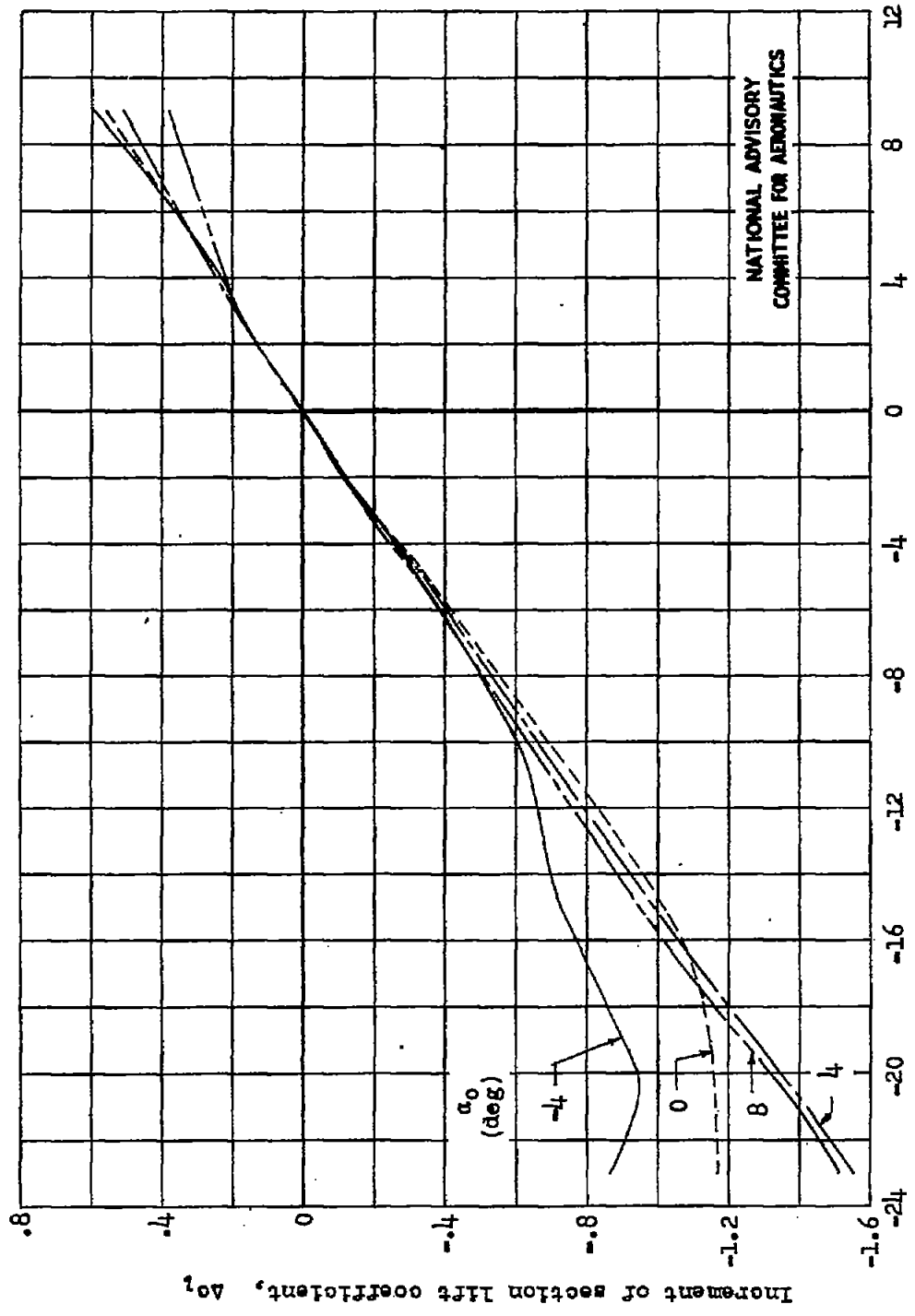

Figure 16.- Variation of Δc_l with δ_e at constant a_o for a low-drag horizontal-tail section equipped with a 0.35c sealed internally balanced elevator. $R = 6 \times 10^6$ (approx.).

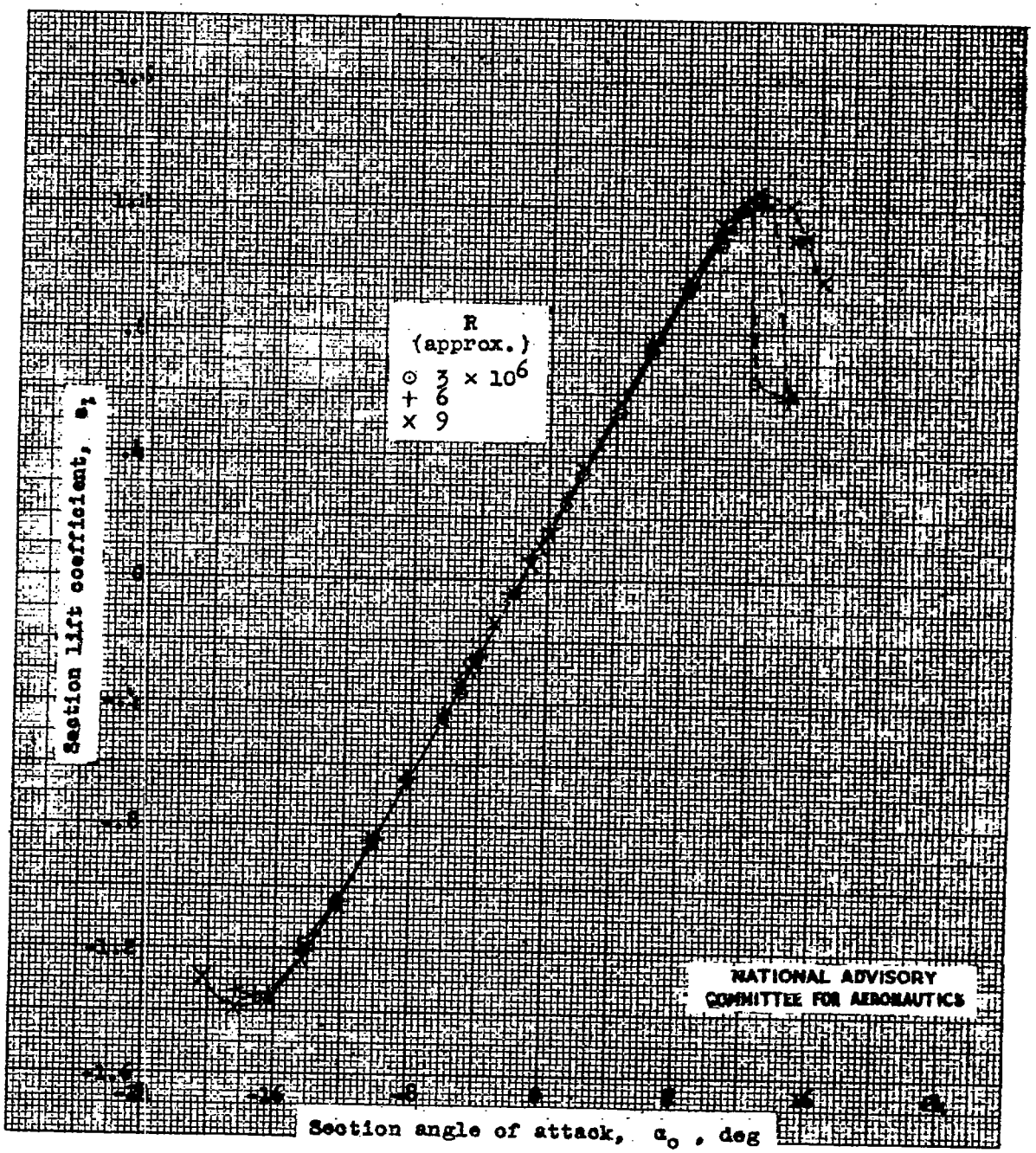

Figure 17.- Lift characteristics of a low-drag horizontal-tail section equipped with a 0.35c sealed internally balanced elevator. $\delta_e = 0^\circ$; test, TDT 581.

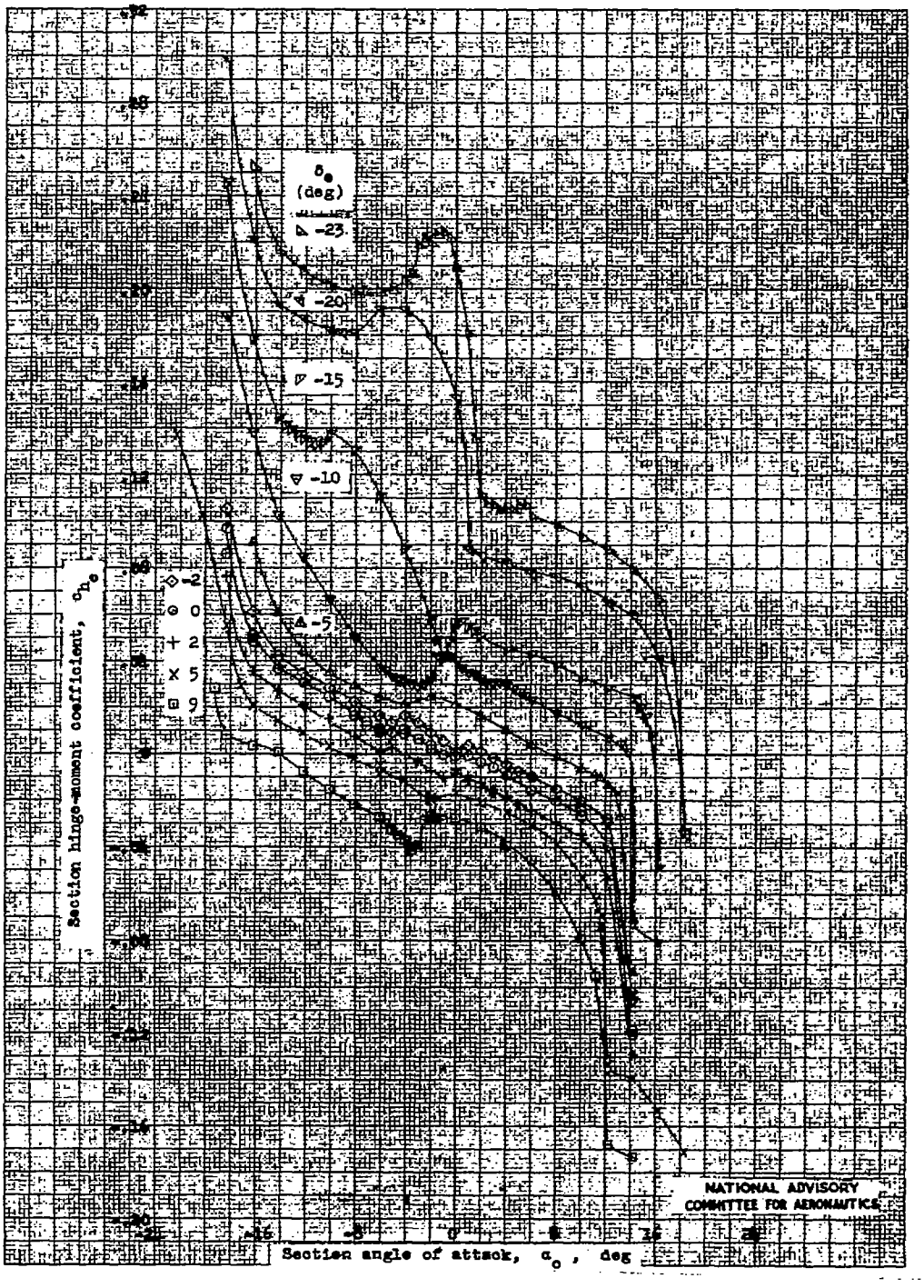

Figure 18.- Hinge-moment characteristics of a 0.35c sealed internally balanced elevator on a low-drag horizontal-tail section. $R = 6 \times 10^6$ (approx.); tests, TDT 581 and 589.

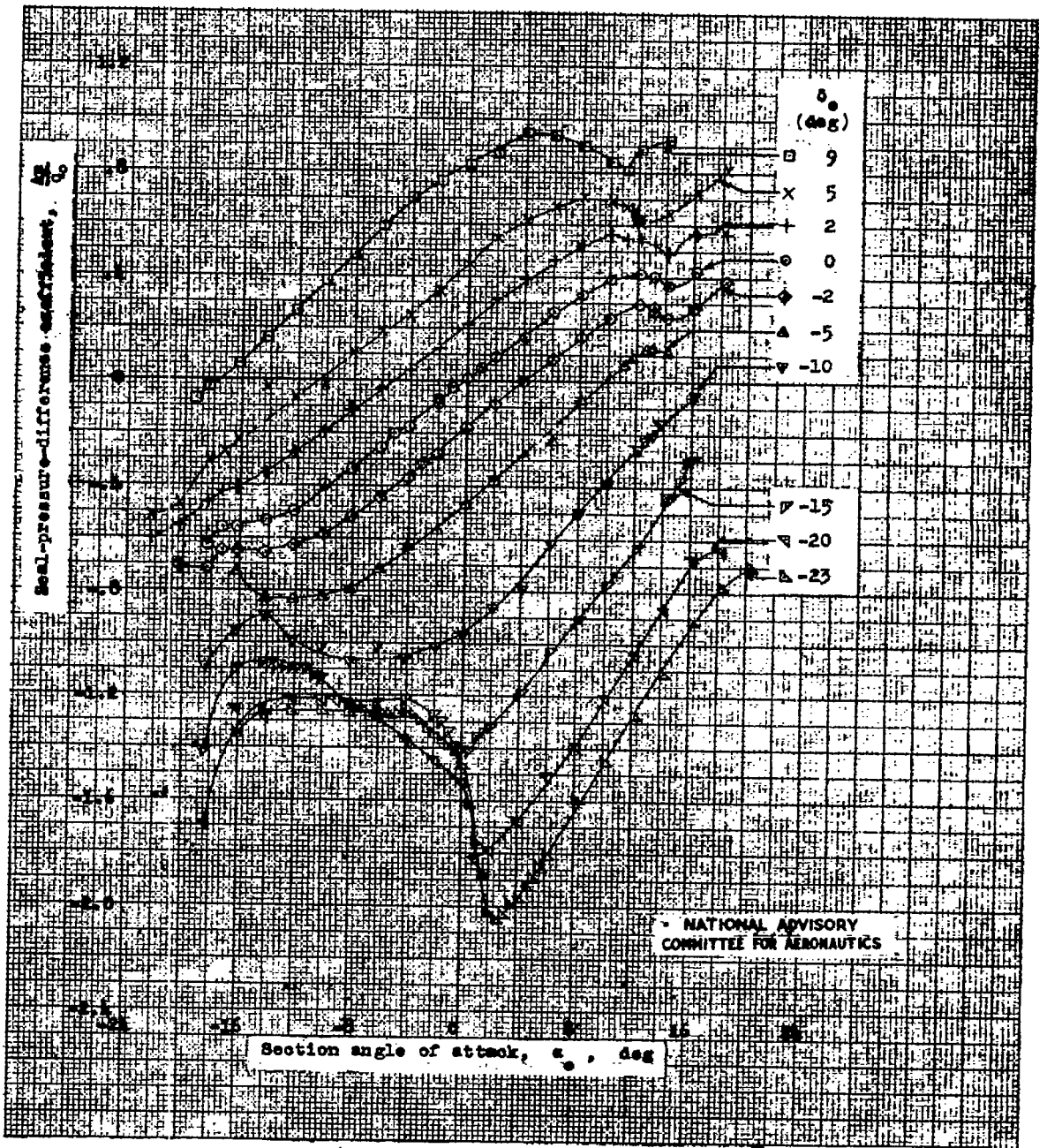

Figure 19.- Variation of $\frac{\Delta p}{q_o}$ with α_o for a 0.35c sealed internally balanced elevator on a low-drag horizontal-tail section. R = 6 x 10^6 (approx.); tests, TDT 581 and 589

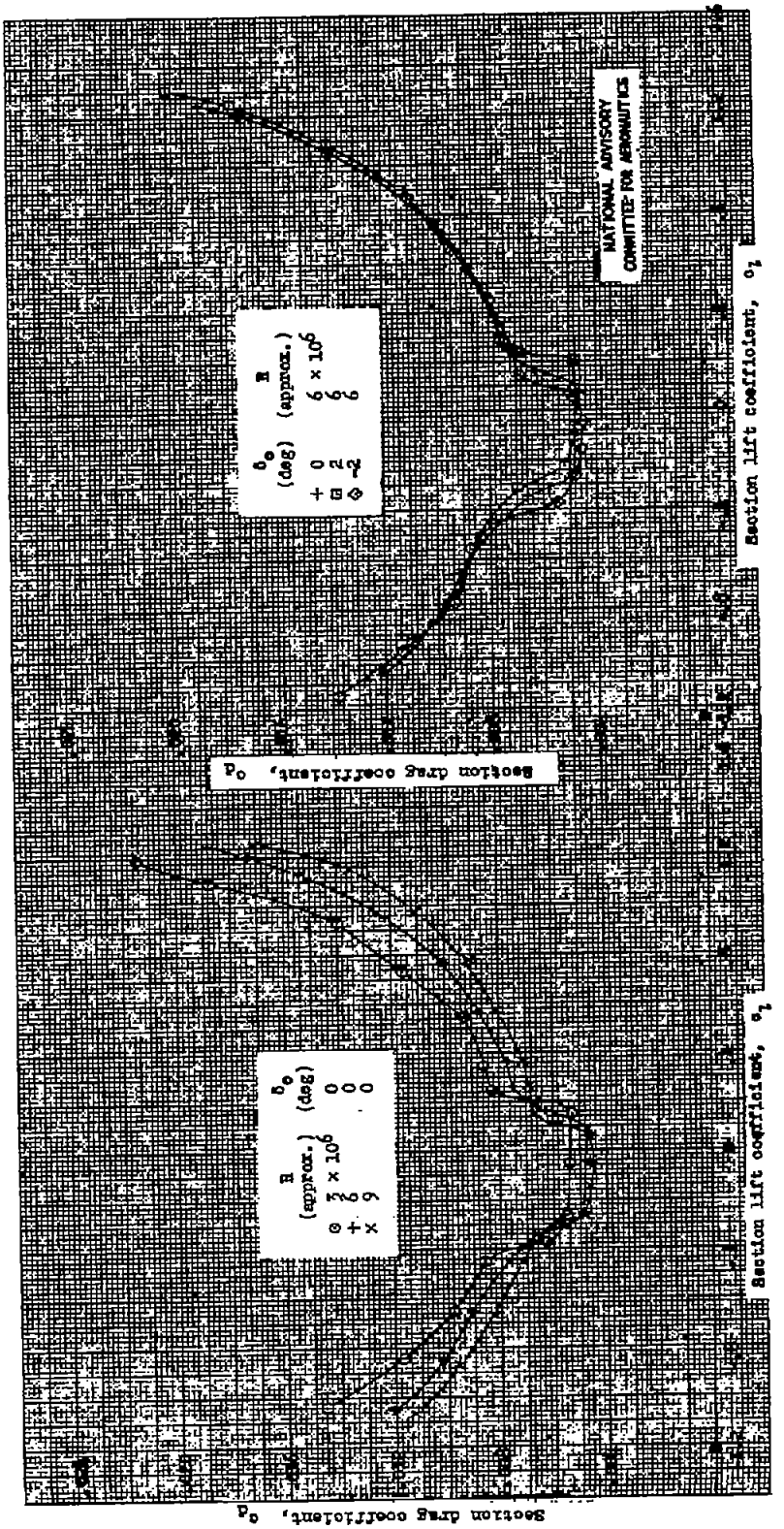

Figure 20.- Drag characteristics of a low-drag horizontal-tail section equipped with a 0.35c sealed internally balanced elevator. Tests, NPL 581 and 589.

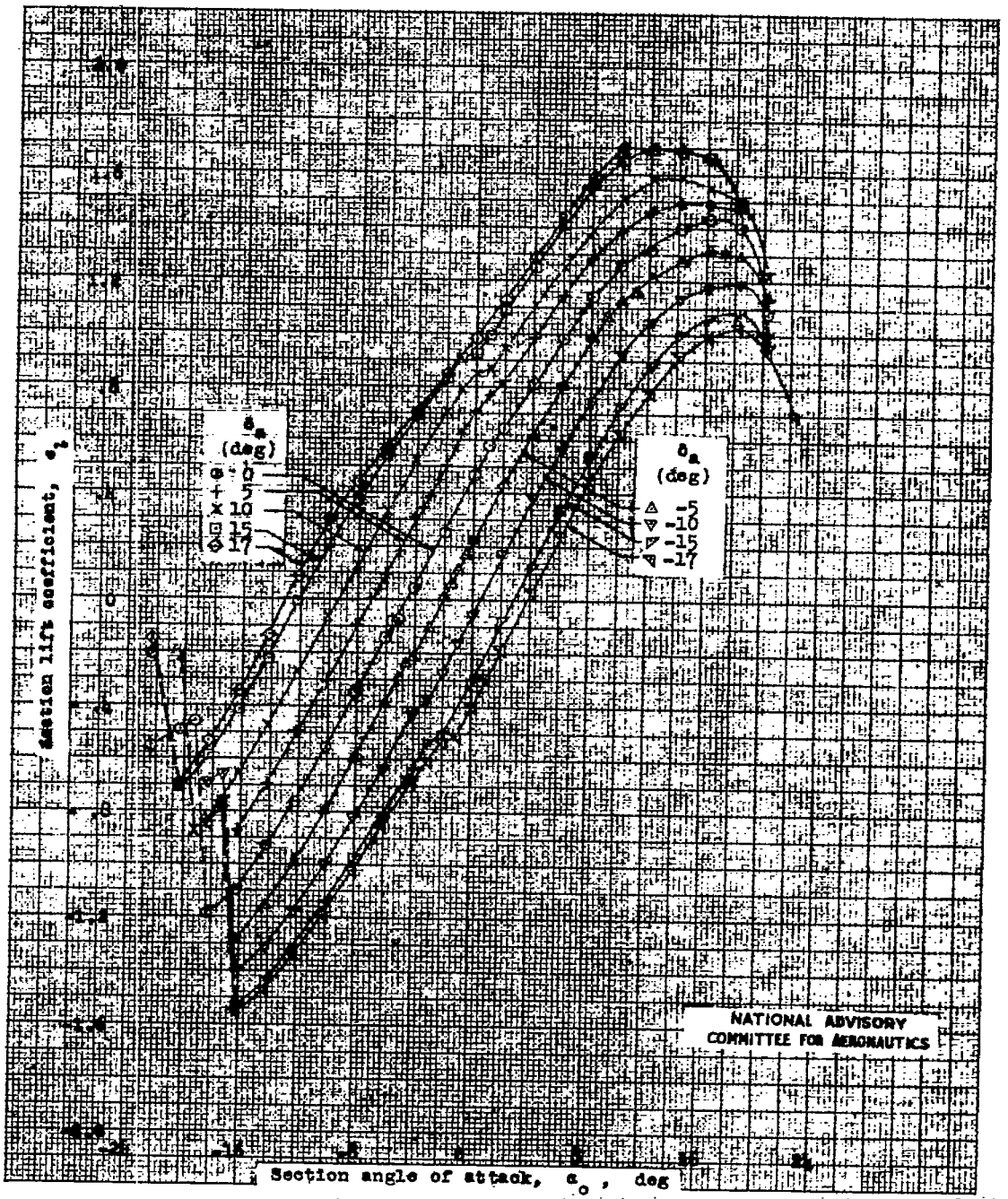

Figure 21.- Lift characteristics of a low-drag wing section equipped with a 0.22c sealed internally balanced aileron. $R = 6 \times 10^6$ (approx.); test, TDT 583.

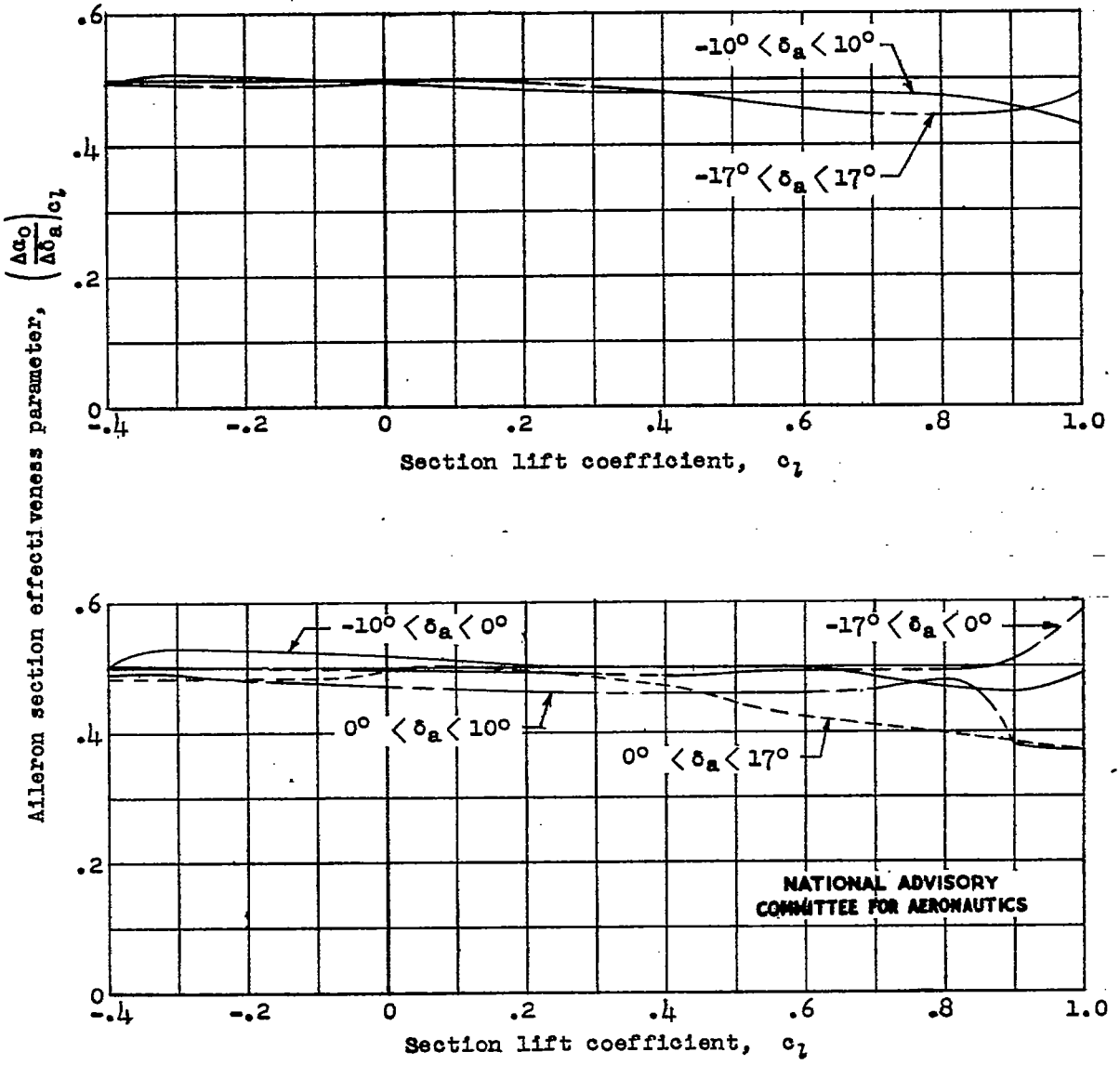

Figure 22.- Variation of $\left(\frac{\Delta a_o}{\Delta \delta_a}\right)_{c_l}$ with c_l for a low-drag wing section equipped with a 0.22c sealed internally balanced aileron. $R = 6 \times 10^6$ (approx.).

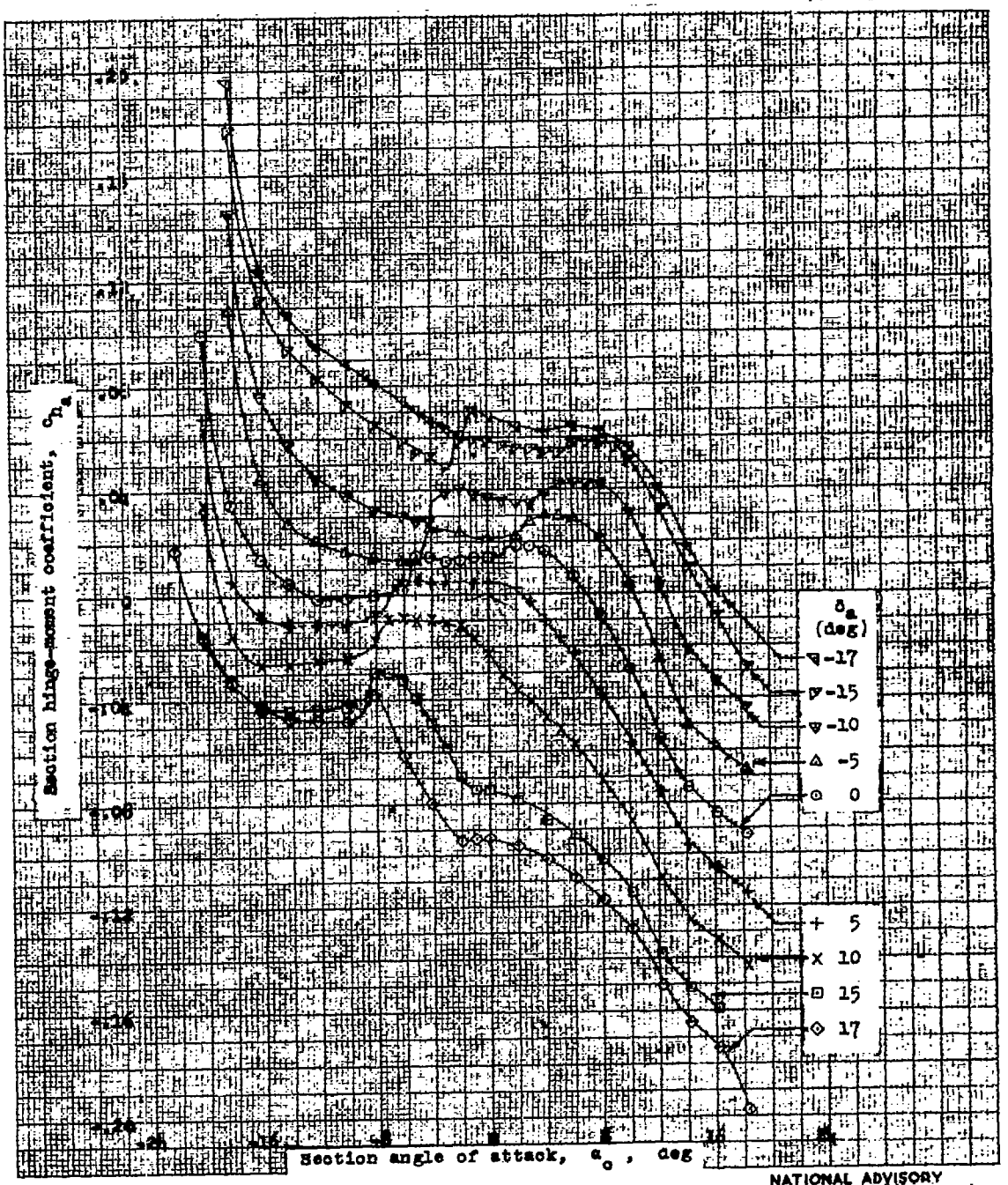

(a) Variation of c_{h_a} with α_o.

Figure 23.- Hinge-moment characteristics of a 0.22c sealed internally balanced aileron on a low-drag wing section. $R = 6 \times 10^6$ (approx.); test, TDT 583.

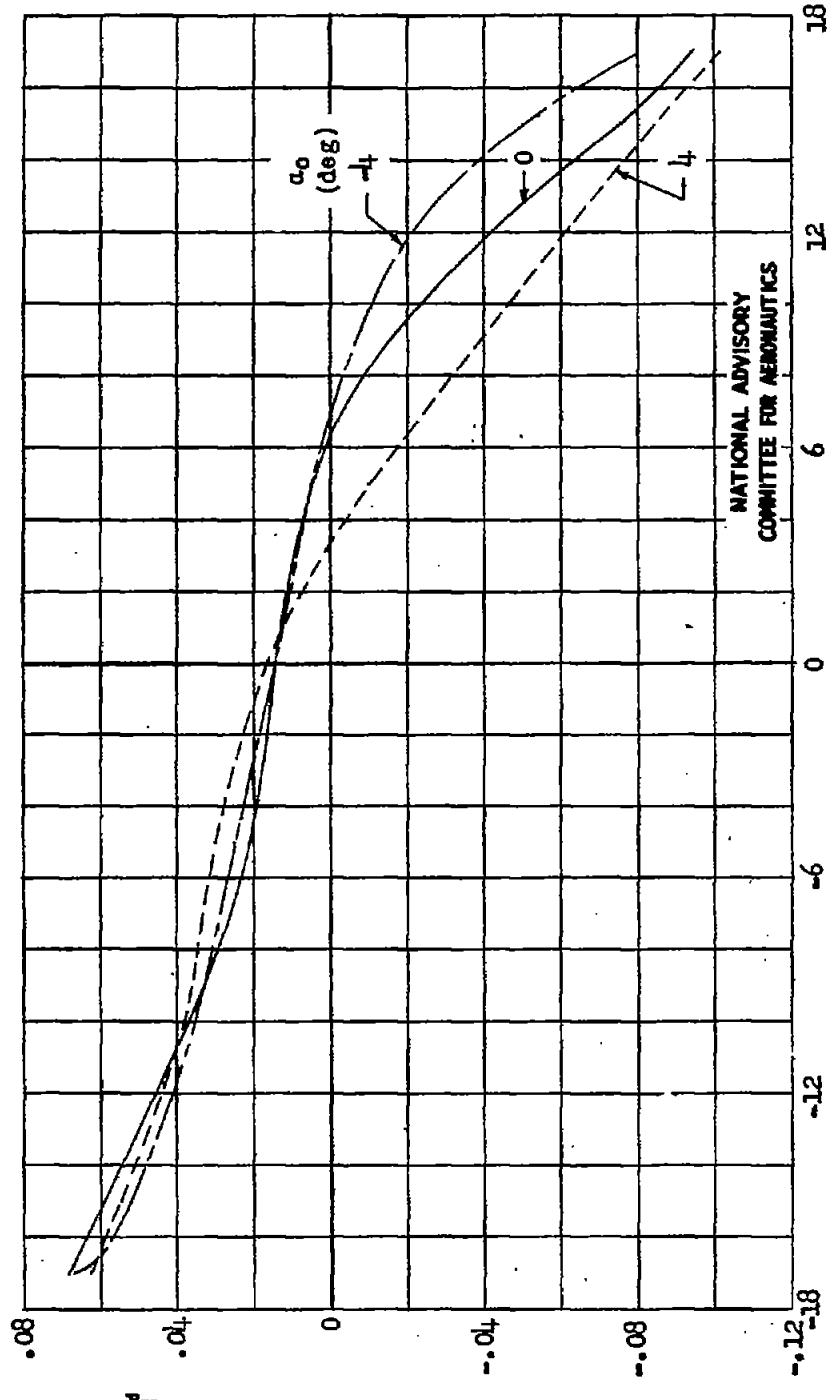

(b) Variation of c_{h_a} with δ_a.

Figure 23.- Concluded.

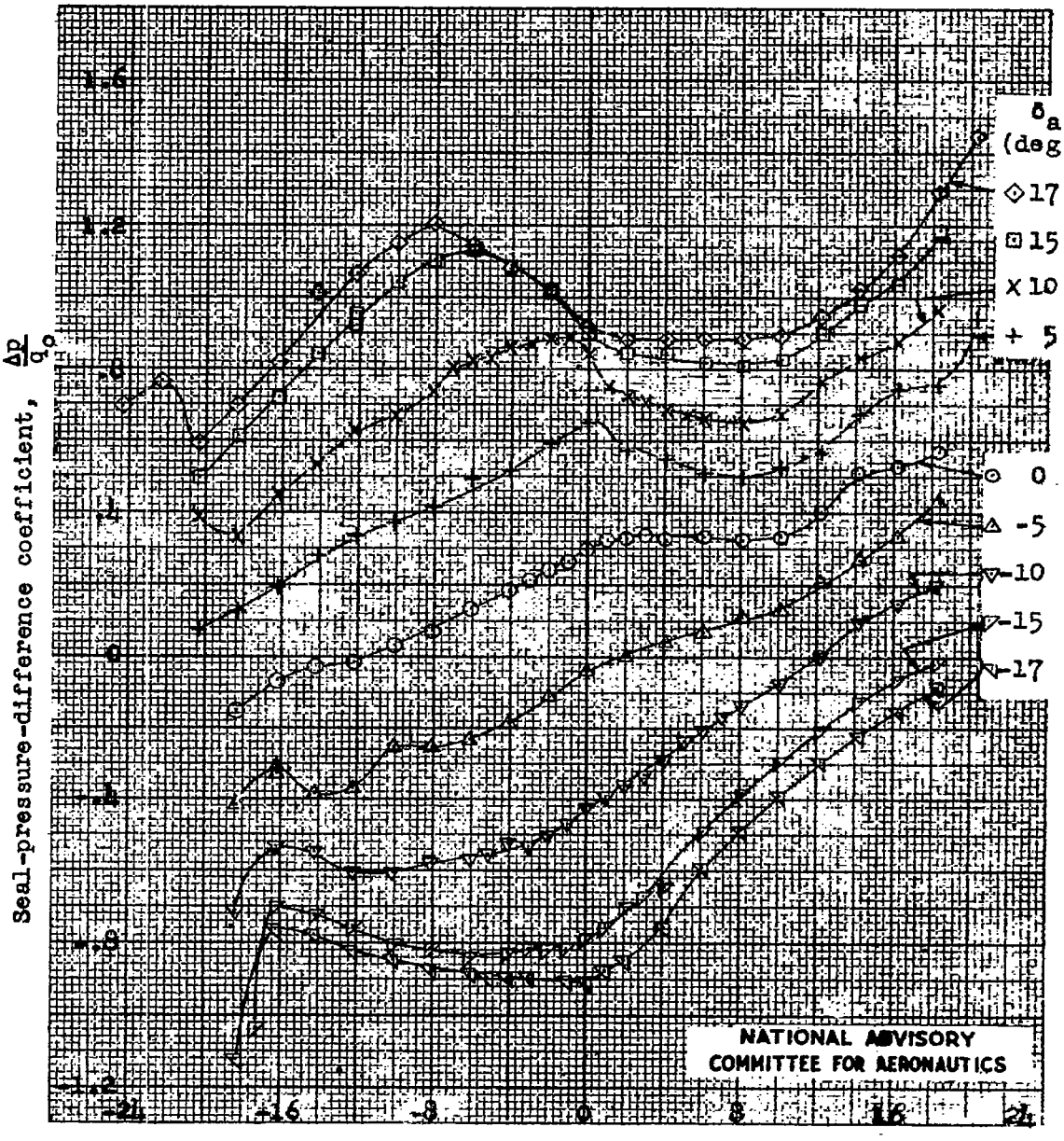

Figure 24.- Variation of $\frac{\Delta p}{q_o}$ with α_o for a 0.22c sealed internally balanced aileron on a low-drag wing section. R = 6 × 10^6 (approx.); test, TDT 583.

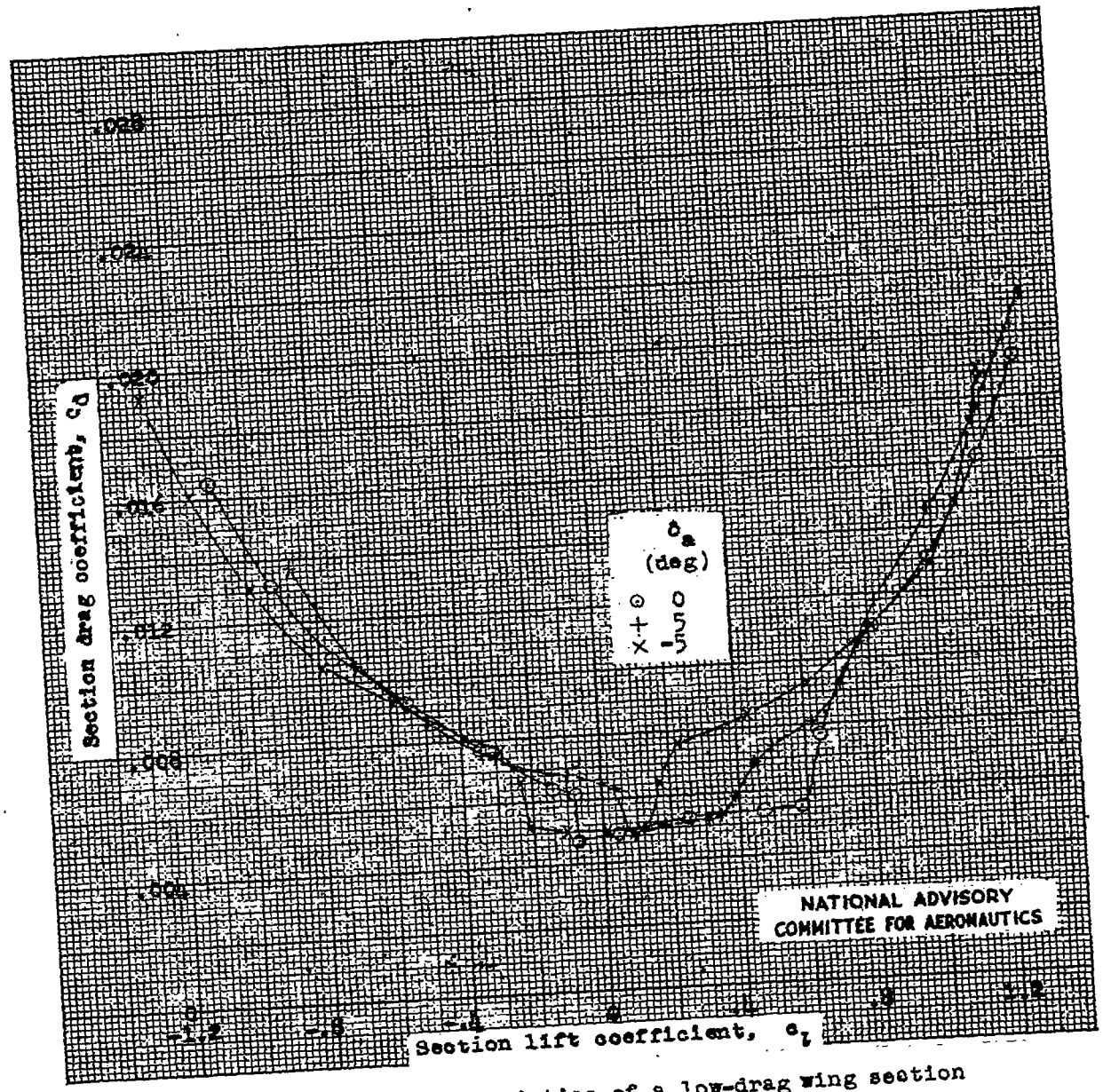

Figure 25.- Drag characteristics of a low-drag wing section equipped with a 0.22c sealed internally balanced aileron. $R = 6 \times 10^6$ (approx.); test, TDT 583.

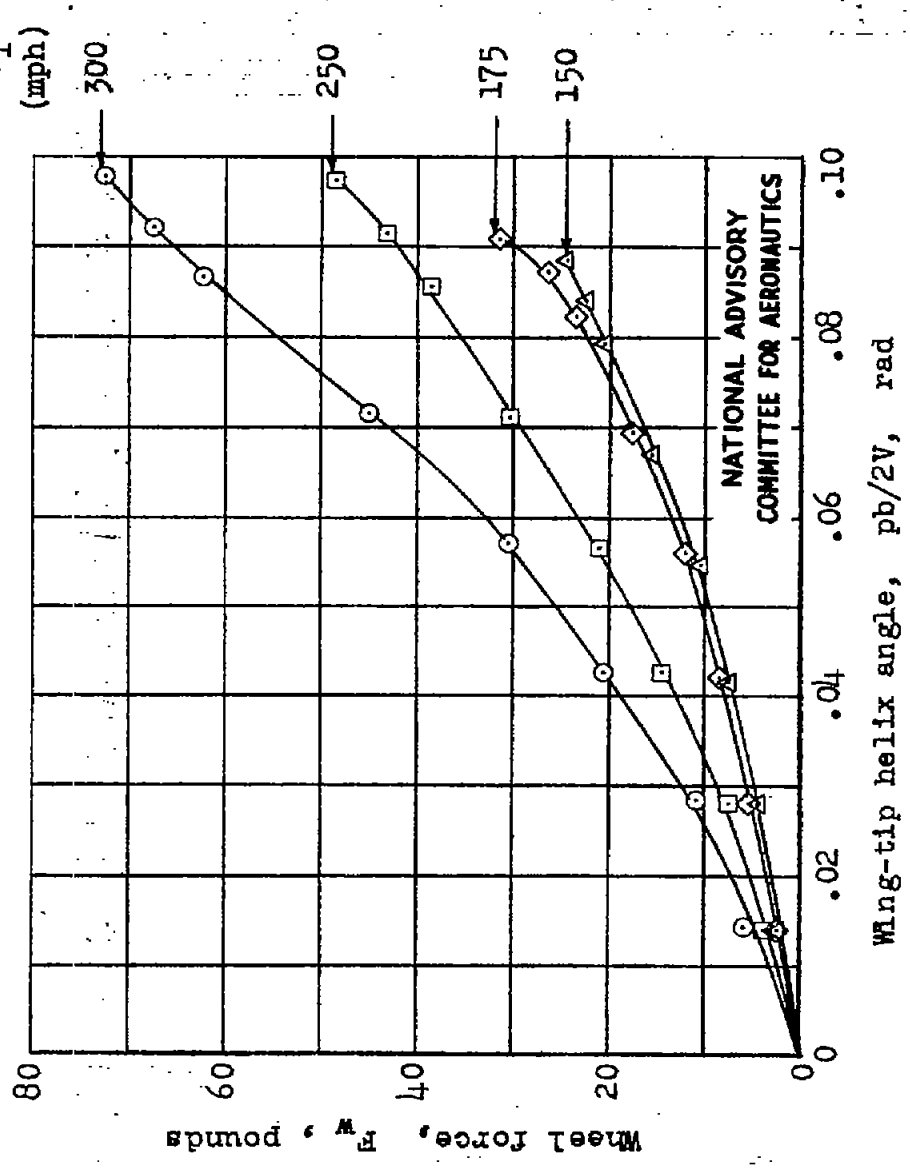

Figure 26.- Variation of aileron wheel force with wing-tip helix angle.